

Helsinki University of Technology

Department of Electrical and Communication Engineering

Laboratory of Electromechanics

Khaled Alkar

**MEASURING POWER LOSSES OF ELECTRICAL STEEL SHEETS
IN ONE- AND TWO-DIMENSIONAL MAGNETIC FIELDS**

Master's thesis submitted for approval for the degree of Master of Science,
Espoo, September 2007

Supervisor

Professor Antero Arkkio, D.Sc. (Tech)

Instructor

Anouar Belahcen D.Sc. (Tech)

Author:	Alkar Khaled Almabrok
Name of the thesis:	MEASURING POWER LOSSES OF ELECTRICAL STEEL SHEETS IN ONE- AND TWO-DIMENSIONAL MAGNETIC FIELDS
Date: September 2009	Number of pages: 71
Department:	Electrical and Communication Engineering (TKK)
Professorship:	S-17 Electrical Engineering (Electromechanics)
Supervisor:	Prof. Antero Arkkio
Instructor:	D.Sc. Anouar Belahcen
<p>Among the electrical machine users and designers, strong interest is shown to reduce the core losses at the design stage. Therefore, a rigorous analysis of the electromagnetic behavior is needed to fulfill such a purpose. Rotational power loss can contribute by a significant amount of the total core losses and, thus, has to be given a thoughtful attention. Mathematical models have been emerging to account for these losses. Yet, these models require validation by measurements and the loss phenomena have to be thoroughly studied. Measuring difficulties are often encountered due to many complications associated with the phenomena.</p> <p>This thesis investigates experimentally the power losses using a modern measuring system in one- and two-dimensional magnetic fields. A measurement technique for rotating flux and magnetic field strength components in electrical steel sheets is presented. The behavior of the power losses in the sheets for one- and two-dimensional excitation fields is studied. A comparison of the power losses under different excitation fields and frequencies is presented. The measuring setup allowed the flux density to reach high values in the used material ($B_y=1.85$ T and $B_x=1.72$ T).</p>	
Keywords:	Power Losses, Rotating Field, Magnetic Measurements, Electrical Steel Sheets.

Preface

This master thesis was carried out at the Laboratory of Electromechanics, Helsinki University of Technology (TKK). The aim of the thesis is to measure the power losses in electrical steel sheets.

I thank my supervisor Professor Antero Arkkio and Professor Asko Niemenmaa for giving me this opportunity to carry out this thesis at the Laboratory.

I give my especial thank to my instructor D.Sc. Anouar Belahcen for his support and help all the time of the work, to Katarzyna Fonteyn to my friend Emad Dlala and his family, and to my friend Najy Elkalashy.

I thank everyone in the Laboratory of Electromechanics at the Helsinki University of Technology for the beautiful times that we spent together.

Many thanks to people that can not be forgotten, especially in this moment, my Libyan, Arab, Finnish, Moslems and international friends for the nice atmosphere.

From the deep part of my heart, I thank my mother Hadhom and father Almabrok, the cause of being here in this world, may Allah bless them both in their graves, my sisters, and brothers for being great supporters during the difficult and good times of the work and of my whole life.

Contents

Preface.....	3
Contents.....	4
List of symbols.....	6
1. Introduction.....	8
1.1 Core losses.....	8
1.2 Hysteresis losses.....	9
1.3 Eddy currents.....	12
1.4 Rotational power losses.....	13
1.5 Motivation and aim of the work.....	14
1.6 Outline of the thesis.....	15
2. Literature review	16
2.1 Methods for measuring the magnetic properties of electrical steel sheets..	16
3. LabView programming	30
3.1. LabView construction.....	30
3.2 Principles of LabView (FPGAs).....	31
3.3 LabView FPGA-based measurement system.....	32
4. Experimental work.....	34
4.1 Description of the measurement setup	34
4.2 LabView FPGA program for measuring power rotational losses.....	37
5. Results.....	43
5.1 1D measurements	43
a. Frequency of 50 Hz.....	43
b. Frequency of 200 Hz.....	52
5.2 2D measurements	54
a. Frequency of 50 Hz.....	54

b. Frequency of 200 Hz.....	63
5.3 Summary table of the results.....	65
6. Conclusion.....	66
6.1 Discussion of the results.....	66
6.2 Measurement setup.....	67
6.3 Importance of the work and suggestions.....	68
7. References.....	69

List of symbols

B	Magnetic Flux Density
H	Magnetic Field Strength
B_x	Magnetic flux density component in x direction
B_y	Magnetic flux density component in y direction
H_x	Magnetic field strength component in x direction
H_y	Magnetic field strength component in y direction
\hat{B}	Maximum value of flux density
\hat{H}	Maximum value of magnetic field strength
B_r	Remanence flux density
H_c	Coercive field
M	Magnetization
α_{ex}	Direction of excitation
μ_0	Vacuum permeability
P_{tot}	Total power losses
P_h	Hysteresis power losses
P_{ed}	Eddy current power losses
P_r	Rotational power losses
ω	Angular frequency
f	Frequency
M_s	Magnetization Saturation
V_{av}	Average Output Voltage
σ	Conductivity

δ	Thickness of the sheet
ρ	Resistivity of the sheet
E	Electrical field strength
J	Electrical current density
$\nabla \times$	Curl operator

Abbreviations

AI	Analog Input
AO	Analog Output
DAQ	Data Acquisition
DMA	Direct Memory Access
FIFO	First In First Out memory
FPGA	Field Programmable Gate Array
INSTR	Instrument
MLQ	Motor Lamination Quality
NO	Non-Oriented
Rd	Rolling Direction
RIO	Reconfigurable Input Output
Td	Transverse Direction
SST	Single Sheet Tester
VCCG	Voltage Controlled Current Generators
VI	Virtual Instrument
1D	One Dimensional
2D	Two Dimensional
3D	Three Dimensional

Chapter 1: Introduction

The growing number of electromechanical devices and the increase of energy consumption in daily lives have become a serious concern for the electrical machine designers. Reducing iron losses is one of the major possibilities to deal with this problem. Scientists and machine designers have found that significant amount of power losses are related to the behavior of magnetic induction in ferromagnetic materials. Thus, understanding and analyzing the behavior of the magnetic field components in the ferromagnetic materials are important factors to determine a suitable material for each application. Studying the characteristics of ferromagnetic materials under magnetic induction may help to design such a material that reduces power losses. Therefore, experimental work to evaluate the power losses in electrical steel sheets and to calculate data that are more realistic is one possible way for machine designers to improve the efficiency.

1.1 Core losses

One of the main elements of the construction of electromechanical devices (electrical motors or/and transformers) is the magnetic material. The main problem lays in the fact that the energy losses within the material are a complex phenomenon. One possible way to explain the mechanism of losses within the magnetic material is as follow.

Within an electrical machine, a piece of ferromagnetic material is composed of many domains; each domain has its own magnetic orientation. When an external magnetic field is applied to a magnetic material, the magnetic material gains energy. This energy is used to reorient the magnetic domains as the external applied magnetic field increases (Del Toro 1985). As shown in Figure 1-1, when an external magnetic field is applied, the domains try to reorganize themselves by expanding if their direction of magnetization is the same as the direction of the applied field. When the magnetic field increases up to a certain value, the direction of magnetization in the domains, changes

and they finally orient themselves in the applied field direction. One point to mention is that two domains are separated by a transition region, also called the Bloch wall, as seen in Figure 1-1. In this region, the magnetic orientation rotates from 0° to 180° ; these changes cause disorganization, which leads to some “clash” between atomic movements within the material. This phenomenon manifests as a heating inside of the magnetic material.

The magnitude and the behavior in time of the external magnetic field have a clear impact on the losses. These losses are known as the core losses or magnetizing losses. Generally, core losses have been divided into two components: hysteresis losses and eddy current losses (Nasar 1995).

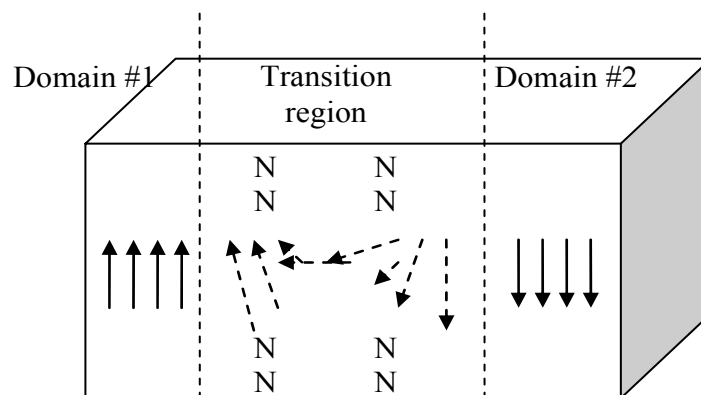


Figure 1-1. Schematic diagram of 180° domain wall (Goodenough 2002).

1.2 Hysteresis losses

When a ferromagnetic material is magnetized starting from the origin P (Figure 1-2), the magnetic field strength is increased and the flux density increases as well. The flux density will not go back to zero when the applied magnetic field is removed, there will be a remanent flux density (B_r). To force the flux density to go back to zero, reverse magnetic field must be applied. The magnetic field strength in this case is called

coercive field(H_c) as shown in Figure 1-2. If the reverse magnetic field continues to increase, the magnetic field strength and the flux density are increased in the other direction until they reach the saturation. The formed curve is called a hysteresis loop.

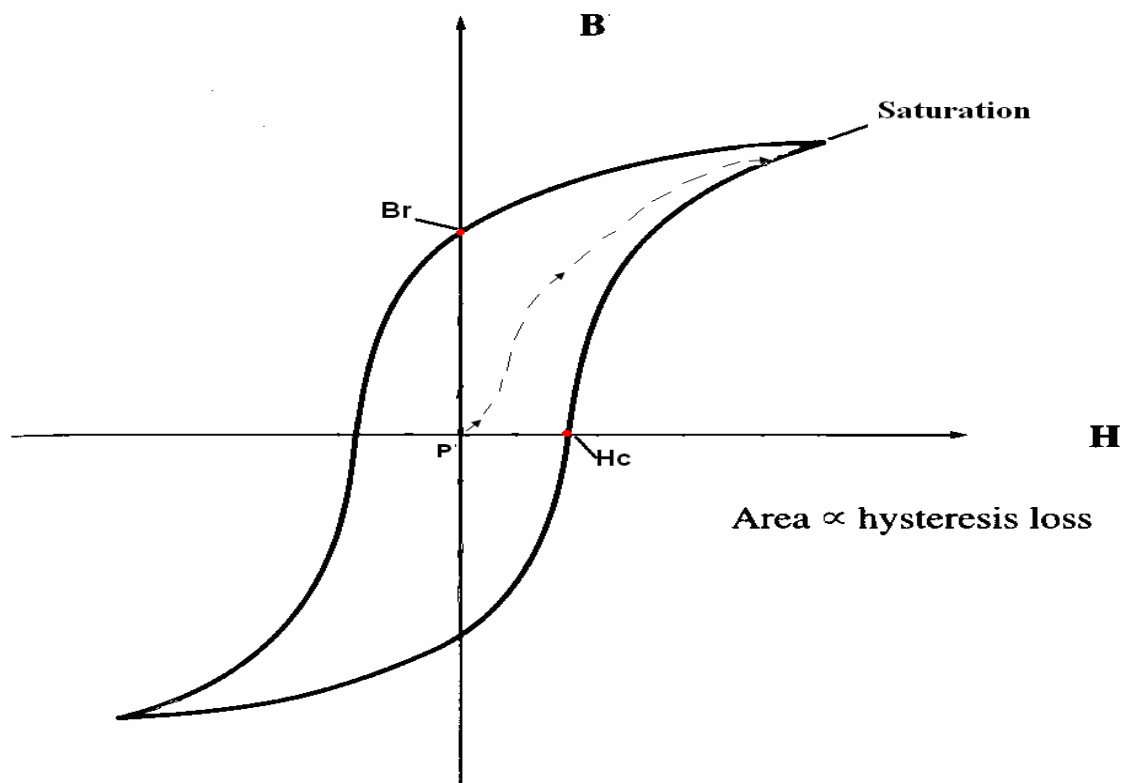


Figure 1-2. The hysteresis loop (Chapman 2005, p.29).

Studying the behavior of the hysteresis loop is significant from the point of view of power losses. This can be seen clearly in Figure 1-3. Energy is dissipated in order to set up the remanent flux. The shaded area between B-H curve and B axis is the work done (Bertotti 1998, p.99).

$$W = \int_0^B \mathbf{H} \cdot d\mathbf{B} \quad \text{J/m}^3 \quad (1)$$

The required energy to 'pump up' the core by moving from $-B_r$ to B_{max} is larger than that it returns from B_{max} to B_r . The difference between those energies is the dissipated energy in the core. This energy loss is dissipated as heat in the core during each cycle of variation of magnetic field strength (\mathbf{H}). In other way, the area of the hysteresis

loop is the energy lost at each cycle. Therefore, the total power losses over one cycle is proportional to enclosed area of the hysteresis loop. Under sinusoidal excitation, the hysteresis losses at each cycle increase with the increase of the frequency, they are also increasing with the increase of the peak value of the flux density (Wiley 1997, p.20).

$$P_h = k_h f (\hat{B}_x)^n \quad \text{W/m}^3 \quad (2)$$

Where k_h depends on the particular core material, P_h are the hysteresis losses, f is the frequency and \hat{B}_x is the peak value of the flux density, n is the Steinmetz exponent.

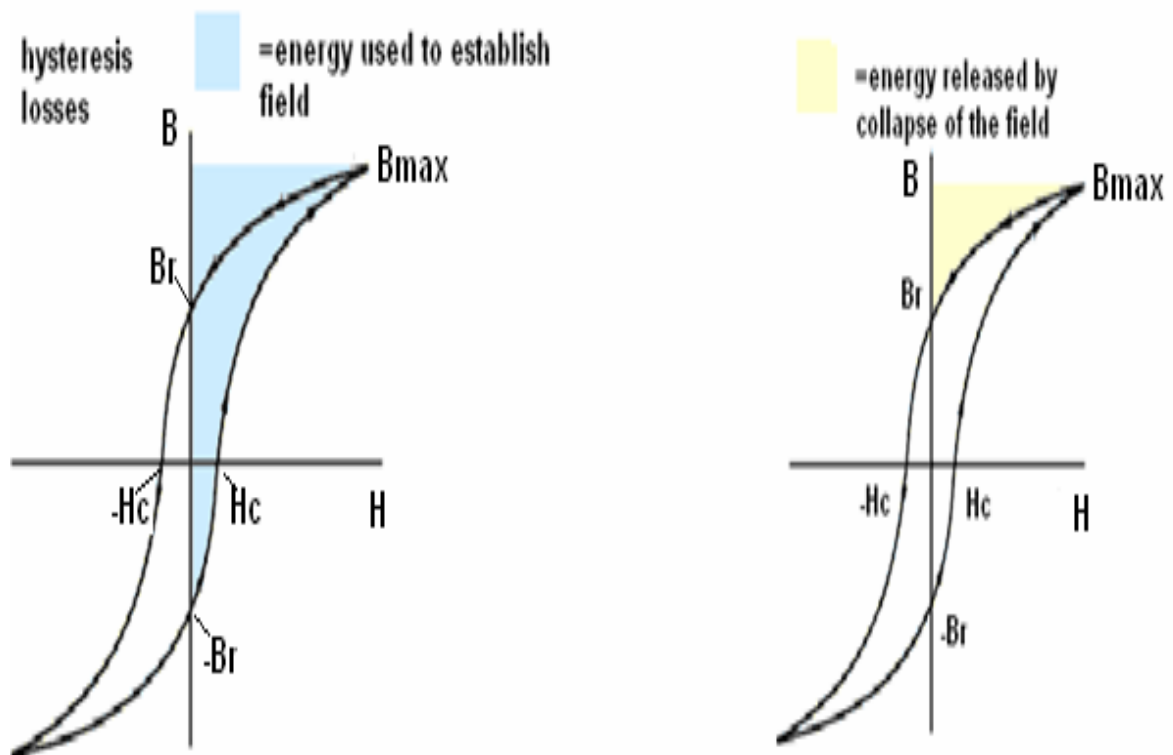


Figure 1-3. The hysteresis loop and the power losses.

1.3 Eddy currents

As the flux changes with time through a conductive material, this change produces electrical field (Bertotti 1998, p.75).

$$\nabla \times \mathbf{E} = \frac{-d\mathbf{B}}{dt} \quad (3)$$

The produced electrical field causes swirls of current within the material as shown in Figure 1-4. These currents are called eddy currents, according to Faraday's law (Chapman 2005, pp. 28-29).

$$\mathbf{J} = \sigma \mathbf{E} \quad (4)$$

In case of alternating field, eddy current losses are assumed to increase proportionally with the square of the frequency, flux density and thickness of the sheet and inversely with the resistivity.

$$P_{ed} \propto (f^2, \mathbf{B}_{max}^2, \frac{\delta^2}{\rho}) \quad (5)$$

δ is the thickness of the sheet

ρ is the resistivity of the sheet material

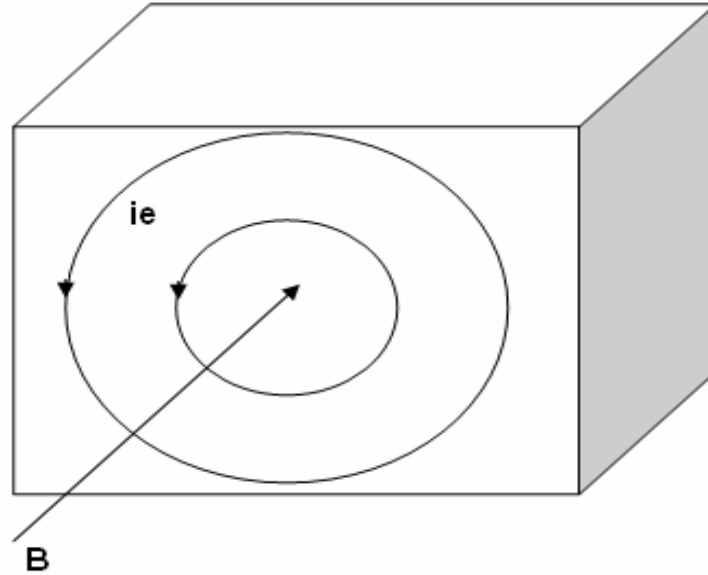


Figure 1-4. Eddy current in electrical steel sheet.

1.4 Rotational power losses

The behavior of the power losses in electrical steel sheets under rotating fields have been experimentally investigated by many researchers. They have found some different phenomena than those, which have been measured under alternating fields. Figure 1-5 shows the behavior of the rotational power losses under different rotating excitation fields in non-oriented sheet sample. As the flux density increases, the rotational power losses increase. At high flux density value near the saturation point, the rotational power losses reach their maximum values. At the saturation point, the power losses stop increasing and start decreasing because the field strength and the flux density become parallel (Brix et al. 1984).

In conclusion, the total power losses in electrical steel sheets are:

$$P_t = \frac{1}{T} \int_0^T (H_x(t) \frac{dB_x(t)}{dt} dt + H_y(t) \frac{dB_y(t)}{dt} dt). \quad \text{W/m}^3 \quad (6)$$

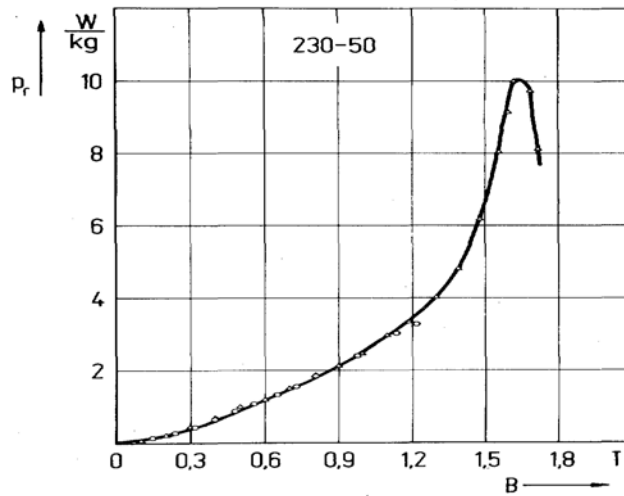


Figure 1-5. The behavior of the rotational power losses with the increase of the flux density B at 50 Hz.

1.5 Motivation and aim of the work

This work aims to measure the power losses in electrical steel sheets under different excitation conditions. First, a special program is built on the LabView FPGA module. This module works with a “National Instrument” card, PCI-7831R, to collect the magnetic field strength and magnetic flux density components ($H_x, H_y, B_x,$ and B_y) from the measurement devices. Second, the power losses in the electrical steel sheets under one- and two-directions excitation are calculated from these measurements.

1.6 Outline of the thesis

In the first chapter, an introduction to the work is presented. The behavior of the magnetic field components in the magnetic materials is studied. In the second chapter, a literature review on various methods for measuring the power losses in magnetic materials is presented. A brief explanation about the methods, which have been used to measure the flux density and magnetic field strength in electrical steel sheets, is presented. In Chapter three, a description of the measuring devices is presented. An introduction to LabView software program and LabView FPGA module and their applications for such measurements is provided. In Chapter four, a measuring setup for the experimental work is introduced. In Chapter five, the results of the measurement are reported and explained. The last chapter contains the conclusions and discussion of the results.

Chapter 2: Literature review

The power losses have been investigated in literature. Scientists have initiated research on this topic since the beginning of the nineteenth century. Since that date, there have been a number of papers on various methods for measuring power losses. The early investigation was concentrating on measuring rotational hysteresis using torque magnetometers.

2.1 Methods for measuring the magnetic properties of electrical steel sheets.

In this part of work, there are many techniques, which have been used for measuring the power losses in the electrical steel sheets. They are explained in the following paragraph.

Young and Schenk (1966) and Boon and Thompson (1965) used a thermal method to measure the power losses in electrical steel sheets. Later, the thermal methods were replaced by other methods, which are mentioned here briefly, for measuring the field quantities B_x , B_y , H_x , and H_y (Sievert 1990, Ymguchi & Narita 1976 and Ishihara & Takahashi 1979).

Werner (1949) was the first who proposed the needle probe method for measuring the magnetic induction quantities in magnetic materials. Stauffer (1952) made the device for using the needle probe method. Field-sensing methods were investigated by Kaplan (1961).

W. Brix et al. (1982) used search coils for measuring the flux density and magnetic field strength in non-oriented silicon iron steel sheets. In this method, they cut the non-oriented steel sheets into cross-shaped samples and magnetically shorted them from their limbs. The magnetizing coils were set on two yokes. The rotational power losses were then calculated from the measured components of the magnetic field vectors in

the non-oriented silicon steel sheets. The measured components were B_x , B_y , H_x , and H_y .

However, some difficulties were raised; for instance, the magnetic field in the center of the sample was not homogenous due to the shape of the sample. In addition, the saturation of the limbs was limited to reach the maximum values of the magnetic induction in the center of the sample.

Few years later, square samples were used instead of cross-shaped samples to reach high values of magnetic field density in the center of the sample. In this technique, the square samples were set into a system of horizontal yokes and the samples were subjected to axis stumps. Magnetizing coils were wound around the stumps to apply a magnetic field to the samples. Needle probes were set into a sensor head for measuring the flux density and field strength components B_x , B_y , H_x , and H_y .

The principle of the needle probe method is based on measuring the potential differences between two points of the surface of the sample on the same side and calculating the flux density. Some problems were also solved such as increasing the magnetic flux density in the sample and reaching more homogenous field in the center of the sample (Brix et al. 1984). However, using the needle probe technique caused some error in measuring the flux density components. In addition, it was sensitive to the noise. To overcome this shortcoming Enokizono et al. (1990) drilled holes in the sample sheet and measured the flux density using search coils wound through these holes.

The needle probe technique has been modified to measure the flux density in electrical steel sheet (Loises and Moses 2001). The principle of this technique was to change the position of the needle tips. The old technique was to set the needle tips on the same side of the sample surface but in the modified technique, the position of the needle tips has changed by putting the sample between them. In this technique, the flux was calculated by integrating the voltage in the measured area between the needle tips and

adding the error due to the flux leakage. The advantage of this technique was to increase the accuracy of the measured rotational power losses, comparing with the traditional needle probe technique. However, the use of this technique was requiring free access to the edge of the sample to make the needed wiring connections. This was difficult to achieve, and put limitations to this technique.

Mori et al. (2005) used a newly developed two-dimensional magnetic measurement method to measure the rotational losses in magnetic core materials. In this method, square samples were used for measuring the rotational power losses at high magnetic flux density. The magnetic field was subjected in both directions; clockwise and anticlockwise. However, the information about power losses as well as the relationship between B and H was not accurate enough and there was a lack of data for the electrical machine designers (Zurek and Meydan 2006).

Burgwin (1936) has suggested the 25cm-Epstein frame technique with double-lapped joints. It has been standardized for many years as magnetic circuit of alternating excitation.

Reyne et al. (1988) have used the so-called 'simplified' Epstein frame to obtain experimental data from samples of ferromagnetic materials. In this method, the Epstein frame as shown in Figure 2-1 contained a sample with the following dimensions; $0.24 \times 0.03 \times 0.0005$ m. The sample was placed in the middle between two horizontal parallel windings, one of them was used to give identical excitation field to the sample and the second to measure the magnetic field density in it. There was also a pickup head with a piezzo-electric transducer at the end of the sample and a yoke made of ferromagnetic material. The pickup head was used to measure the deformation in the sample. In this technique, the results have shown deformation in the sample. The deformation depends on the value of the flux density.

However, the overlapping of the sheets at the corners in the Epstein frame may lead to inhomogeneity of the flux. The difficulty of specimen preparation in the Epstein procedure caused strong need for alternatives.

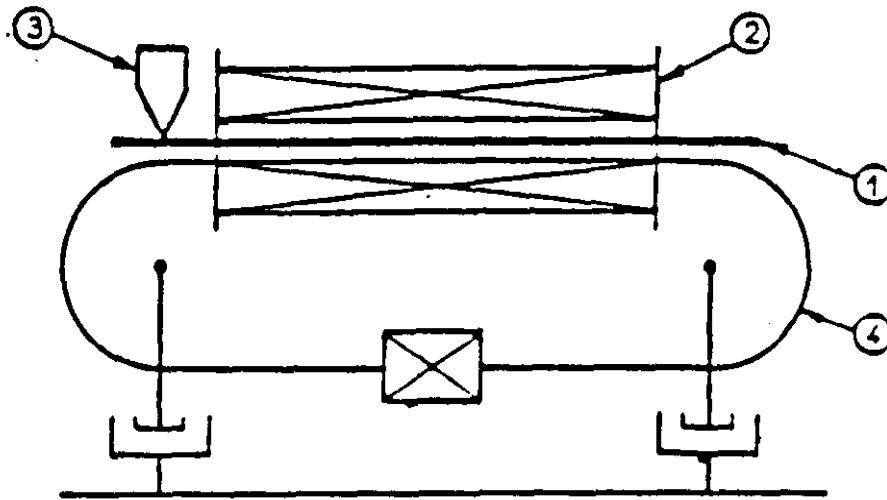


Figure 2-1. "Simplified" Epstein Frame.

- 1- Sample (0.24×0.03×0.0005) m.
- 2- Windings.
- 3- Pickup head with a piezzo-electric transducer.
- 4- Ferromagnetic yoke.

Moses et al. (1972) have studied the power losses and the flux distribution in the transformer core. The basic apparatus included three main parts as shown in Figure 2-2. The first part was a three-phase core that was constructed from lamination of 3.2% Goss-oriented silicon iron. The area of the core was 1.8 m × 0.9 m with 0.15 m thick lamination. There were two parallel clamping plates, which were used to support the yokes. At each leg of the core, there was a fixed bolt and a washer to fasten the plates. Into each leg, there were ten laminations and a paper between them to avoid unnecessary bending. Moreover, there was a three-phase source with 50 Hz in order to produce flux densities up to 1.6 T in the core. Regulating the primary voltage helped to

obtain uniform flux densities in the legs. The second part was used to calculate the total flux density in each limb from the secondary windings. Search coils were wound around the yoke and around the clamping plate to measure the flux density distribution.

The peak flux density \hat{B} in the limb was calculated as:

$$\hat{B} = \frac{V_{av}}{200NA} [T] \quad (7)$$

where V_{av} is the average output voltage (V), N is the number of secondary coil turns, and A is the cross-sectional area of the core (m^2).

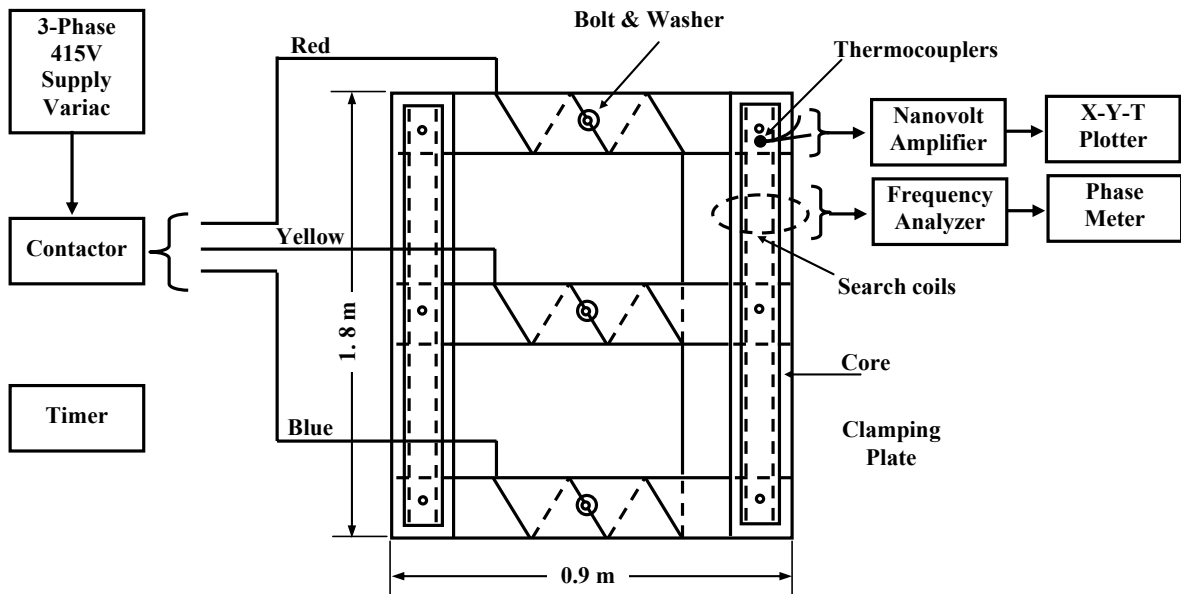


Figure 2-2. Schematic diagram of the three-phase core and measuring equipment.

The last part was used to measure the local losses from the generated heat. In this part, small areas of laminations were used as samples to measure the power losses. The principle of this technique was to measure the power losses as a proportional function to the rise rate of the temperature. It was done by miniature thermocouples, which were set on the yoke and on the limb laminations. In this technique, the results have shown the distribution of power losses in the measured points as well as the difference between the losses at both edges of the yoke laminations. The highest value of the power losses was found in the inner edges of the yoke and of the limbs due to the third

harmonic of the flux density component. However, the core had to be cooled at least ten minutes after each measurement. Therefore, the cooling time caused cooling errors. These errors influenced the accuracy of power losses measurements.

Few years later, Ramos and Girao (1991) used an automated measurement system to study the behavior of ferromagnetic materials subjected to magnetic field. In this technique, the apparatus was consisting of a square yoke as shown in Figure 2-3 and two excitation coils with 1000 turns each. They were wound around four limbs. The limbs were mounted on a cross-shaped sample, which was placed in the center of the yoke. Two orthogonal sensing coils were wound around the four stumps of the sample to measure the flux density components. The number of sensing coil turns was 180 for each. In this measurement, the magnetic field was acquired by H_y sensing coil (10 000 turns with enclosed area $22 \times 0.5 \text{ mm}^2$) which was set on top of the sample. Two voltage controlled current generators (VCCG) were used to feed the excitation coils. IEEE-488 remote controlled switch-control unit was used to get different polarities. The test apparatus was fed through two digital-to-analog converters and analog integrator. The Analog integrator was used to get the values of the magnetic induction components B_x and B_y inside of the sample.

In this method, computed and measured hysteresis loops were compared in a non-oriented silicon iron sample. The results of the measurements were close to the computational Preisach model's results. However, the measurements were only done in one-direction and the characteristics of the material in two-directions still needed further work. The methods have presented the hysteresis loops only in the saturation case. They have not explained the characteristic of the material under different flux densities.

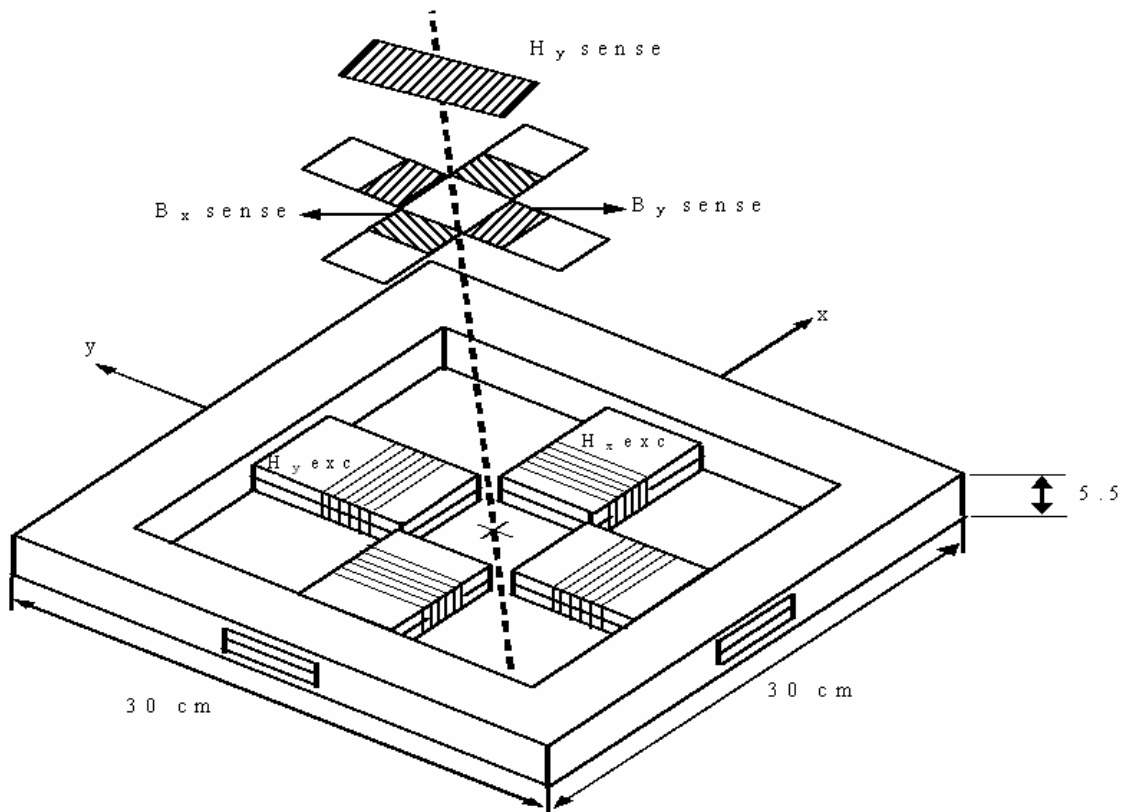


Figure 2-3. Test apparatus of the automated measurement system.

Enokizono and Tanabe (1997) have measured the rotational losses using a simplified loss tester. In this technique, the apparatus consisted of two U-shaped yokes that were set in the x- and y- directions as shown in Figure 2-4. A non-oriented silicon steel sheet (H50, 0.5 mm thickness) was the desired sample for testing. The sample was placed above the four legs of the yokes. The exciting coils (coil-A) were wound at the end of each leg and two exciting coils (coil-B) in the center of the yokes. The field strength was measured by two H-coils, they were placed at the top and the bottom of the sample. B-coils were wound around the sample through four 0.6 mm holes in x- and y- direction, and the distance between each two holes in the same direction was 24 mm. B-needles were subjected to both ends of the B-coils from both faces of the sample to measure the flux density. In this technique, the flux density in the sample was measured by A and B sensors as shown in Figure 2-4 and the rotational losses were calculated from the measured results. The measurements were done under different

frequencies (10-100 Hz). However, these measurements were not accurate due to the variation of the flux that is caused by eddy currents in different area of the sample, the flux did not pass uniformly in the sample due to the excitation coil positions in the yoke and the construction of yoke itself. Moreover, the measurements were done under low flux density 1.0 T and nowadays applications need measurements with higher flux densities and higher frequencies.

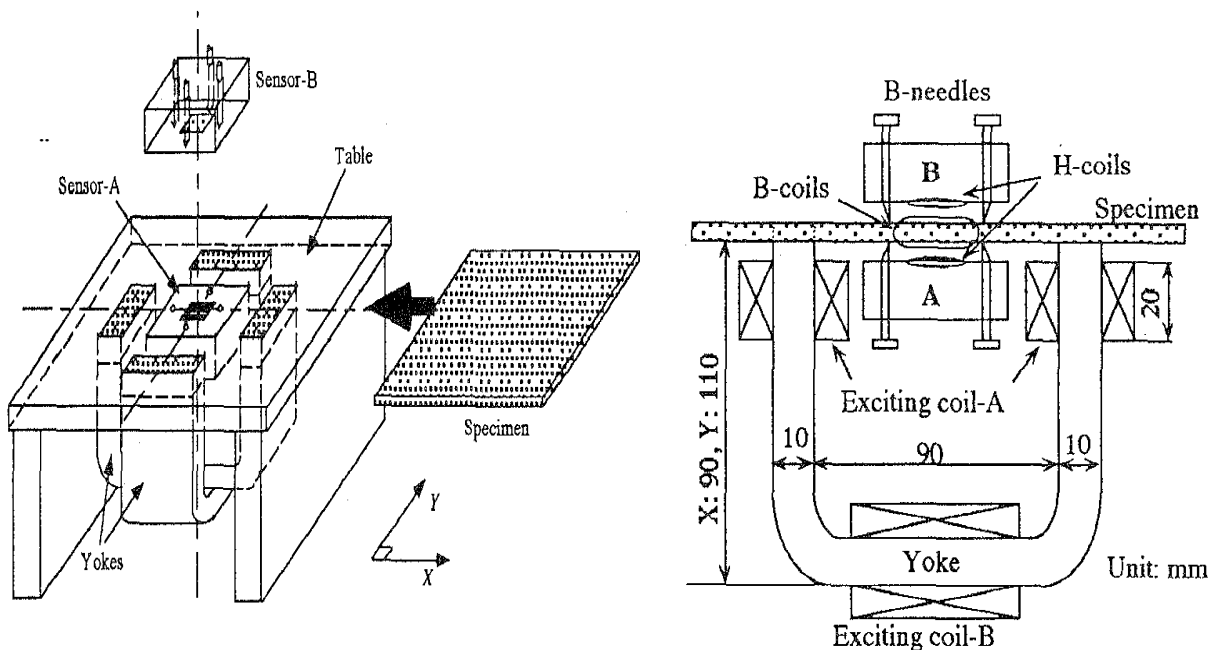


Figure 2-4. Structure of simplified loss tester.

Ivanyi and Pfitzner (1998) presented 2D and 3D models to examine the behavior of rotational field in a single hexagonal sheet tester of anisotropic material. In this model, numerical field analysis was used to estimate eddy currents and magnetic hysteresis. The interaction between the sample and magnetic poles was neglected. The sample was in hexagonal form with 80 mm of each edge as shown in Figure 2-5.

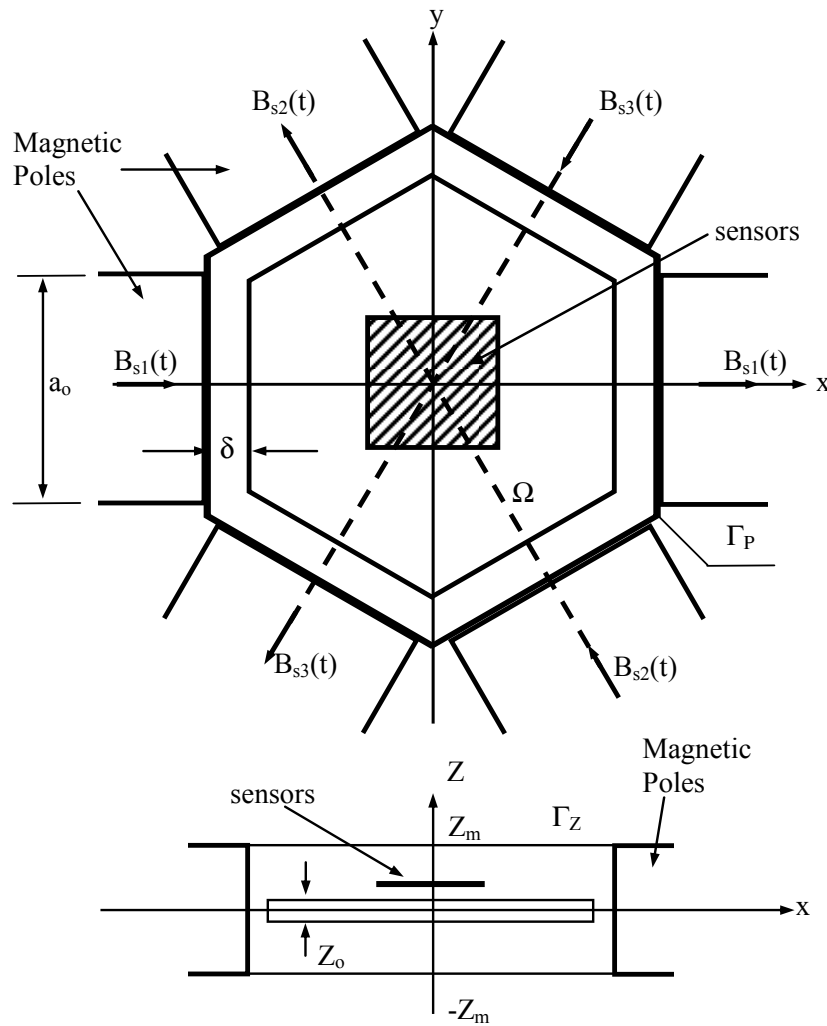


Figure 2-5. The arrangement with the magnetic poles.

The thickness of the plate was 0.35 mm, the distance between the edge of the sample and the poles was 0.35 mm, and the conductivity of the material was $\sigma = 2.1 \times 10^6$ S/m. Sensor coils were used to simulate the magnetic field. They were set on the top center region of the sample of length $l_o = 50$ mm. The supplying source was a balanced three-phase voltage to generate the rotating magnetic field through the laminated magnetic poles. In this model, x-axis was selected to coincide with the rolling direction and the other two axes were selected as the transverse direction. After identifying the model parameters in both directions, the model was able to calculate the components of

vector hysteresis. In 2D model, the results have shown the hysteresis loops in rolling and transverse directions. In the rolling direction, the irreversible rotational magnetization occurred at low magnetic field values, but in the transverse direction, it only occurred at high field values due to the anisotropic properties of the material (Ivanyi and Pfitzner 1998, Yamamoto et al. 1997). Moreover, the flux density in the center of the sample was low due to the strong effect of eddy currents. In 3D model, the results have shown a high flux density in the center of the sample due to the reduction of the eddy current. These results were obtained only by 3D numerical field analysis. Thus, real experiments had to be done. Moreover, the accuracy of the results especially in the 2D model was affected by the thickness of the magnetic sample (Ivanyi and Pfitzner 1998).

Stranges and Findlay (2000) described a method for measuring the rotational iron losses in electrical steel sheet. In this technique, the setup device was consisting of a horizontal yoke with 8 legs which were joined as a square shape and each leg was 50 mm wide and 30 mm thick as shown in Figure 2-6. Between each two legs of the yoke, there was a pole piece constructed. One end of the pole piece was joined between the legs and the other end was subjected to the center of the yoke where 80 mm × 80 mm square samples were placed. Energizing coils were wound around each pole piece to produce induction field in the sample. In this technique, the flux density was measured using search coils, which were wound through drilled holes in the sample. The field sensing system was used to measure the flux density components (B_x , B_y) and the magnetic field components (H_x , H_y) in the sample as shown in Figure 2-6. The field sensing system consisted of x and y coils that were used to measure the flux density components from the sample. They were connected through amplifiers and Keithley electrometers (AWFG D/A) to a computer. The Keithley electrometer was used to convert the flux to voltage and supply it to the computer. The gradient magnetic field strength in both directions, H_x and H_y , was measured by using tangential H-coils. The power losses were calculated from the components of the magnetic field strength and flux density.

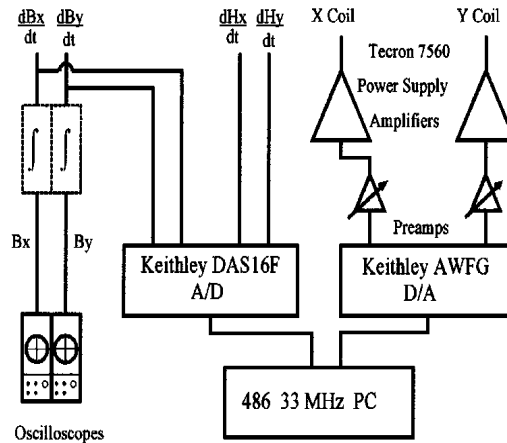
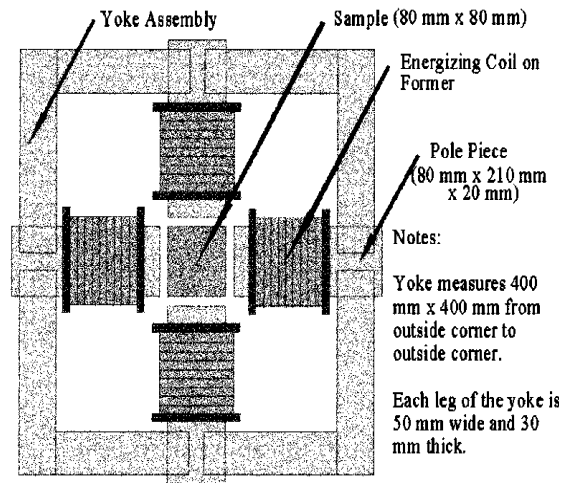


Figure 2-6. Horizontal yoke and field sensing system (Stranges and Findlay 2000).

In this technique, the team investigated various kinds of magnetic materials and divided them to two groups of measurements.

The first measurements included non-oriented steel A, 0.635 mm thick 1.75% silicon steel, non-oriented steel B, 0.48 mm thick 2.70% silicon steel, Non-oriented steel C, 0.635 mm thick 2.75% silicon 0.35% aluminum and 17% manganese steel, and finally non-oriented steel D, 0.48 mm thick 2.70% silicon and 0.15% manganese steel. The

rotational losses for the materials were measured in clockwise and anticlockwise directions and the divergence emerged between flux densities 0.8 to 1.0 T.

In the second measurements, Low Alloy Motor Lamination Quality (MLQ) steels were used. The nominal thickness for all grades was 0.635 mm. MLQ steel A has a nominal alloy content of 0.35% manganese. MLQ steel B has a nominal alloy content of 0.60% silicon and 0.35% manganese and MLQ steel C has a nominal alloy content of 0.75% silicon and 0.65% manganese. In these measurements, the rotational losses were measured in both directions clockwise and anticlockwise and the divergence emerged at different range of flux densities from 0.9 to 1.2 T.

In the measurements for all materials, the results have shown some effects of the composition of the sheet and its thickness on rotational power losses. Moreover, the rotational losses could be estimated under low flux densities. However, the rotational power losses were overestimated due to the saturation of the material at high flux densities in clockwise and anticlockwise directions.

Using square single sheets, the previous methods have faced some difficulties such as high magnetic flux density and wide area of uniform magnetic flux density with sinusoidal waveform control. The next method deals with those issues.

Mori et al. (2005) measured the rotational magnetic losses in magnetic core materials at high magnetic flux density in clockwise and anticlockwise directions. In this technique, three kinds of non-oriented electrical steel sheets were studied. These kinds were 50A230, 50A470, and 50A1300. The apparatus was consisting of four vertical yokes with slits and exciting coil frames in x and y directions around a sample as shown in Figure 2-7. The apparatus was used to measure 2D magnetic properties in the sample under high flux density (1.5 T). The slits in the yokes were used to increase the area where the flux density was uniform, which was over 40 mm².

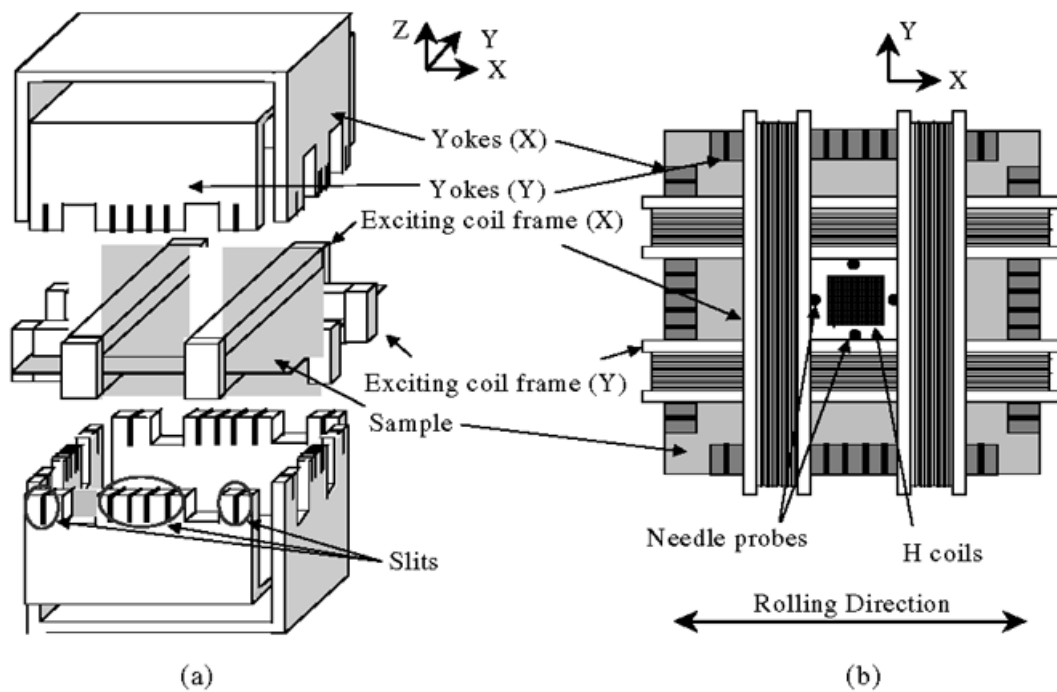


Figure 2-7. Two-dimensional measurement setup. (a) Structure of yokes with slits and exciting coil frames. (b) Top view of B and H sensing devices.

In this technique, magnetic circuits were used to magnetize a sample of size 170 mm^2 in both x and y direction, which were the rolling and transverse directions respectively. The magnetizing coils were wound around the sample. The flux density components B_x and B_y were measured by needle probes and the field strength components H_x and H_y were measured by H-coils. Figure 2-8 shows a Block Diagram for the digital measurement system. The measurement system consisted of a computer with GP-IB interface between the hardware and software, one function synthesizer, two power amplifiers, and one wave memory. The function synthesizer was used to generate arbitrary waveforms in the computer and to excite the samples through two amplifiers that were connected to exciting coils in x and y directions. “Iterative Feedback” was used to get a sinusoidal flux density condition. The “Iterative Feedback” was done by amplifying the output voltages of the needle probes and H-coils and input them to the computer in order to get the B-H loops.

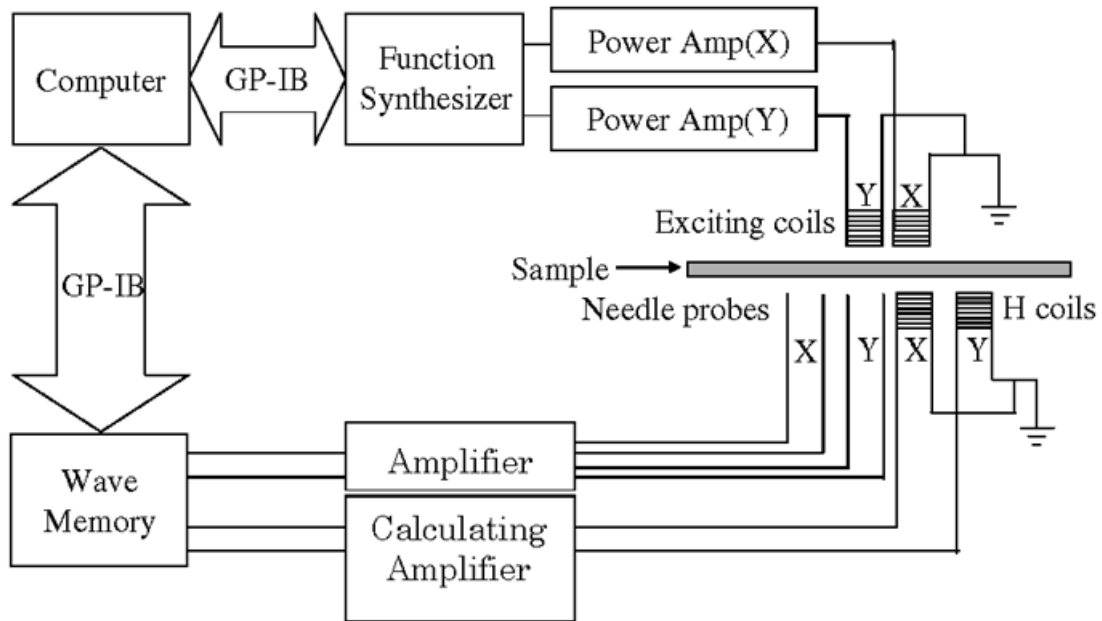


Figure 2-8. The Block Diagram for digital measurement system.

Finally, the results have shown the rotational losses of the samples in clockwise and anticlockwise directions at maximum flux density $B_{max} = 1.7$ T and the average of the losses between the two directions. The losses in clockwise direction were increased with increasing \hat{B} over 1.7 T but they were reduced in anticlockwise direction. However, the problem was in the difference between the measured power losses in both directions.

Finally, under 2D magnetic flux conditions no international standard exists to define the power losses (Stranges and Findlay 2000).

Chapter 3: LabView programming

LabView (Laboratory Virtual Instrumentation Engineering Workbench) is a platform and development environment for visual programming language from National Instruments. LabView is a program development application like other programs such as FORTRAN or C. LabVIEW uses a graphical programming language, which is very powerful to build programs in Block Diagram form, while FORTRAN or C programs use text-based languages to create lines of code. LabView program is called virtual instrument (VI) because its appearance and operation can imitate an actual instrument. National Instruments (NI) LabView has many versions. In this work, Version 8.20 of LabView is used. It is designed for acquiring, analyzing, and presenting data from the unit under test. It is also used for solving engineering and scientific problems. LabView can operate and interface with various hardware devices through different kinds of cards. In these measurements, the used interface is NI-7831R card. With LabView and NI-7831R card, a complete interface between the hardware devices and the computer becomes possible.

3.1 LabView construction

LabView programs are constructed of three main parts; the Front Panel, the Block Diagram and the Icon/Connector.

The Front Panel is built by; Knobs, Push Buttons, Graphs, Controls and Indicators. The users can easily control the running program through these elements on the Front Panel. The Block Diagram contains all the needed functions for building such a program. These functions appear as terminals on the Block Diagram with their own nodes that can be connected to each other through suitable wires and according to the desired control of the program (LabView user manual 2003).

LabView includes three modules, which are Field Programmable Gate Arrays (FPGAs) module, Real-Time module and Simulation module. For our measurements, the FPGA module was the suitable one.

There are many benefits behind selecting LabView FPGA module and these are;

- 1- The configuration for the analog and digital inputs and outputs does not require from users skills of low-level design language.
- 2- It is possible to build or develop an own code easily in the Front Panel and Block Diagram in FPGA VI software which works on operating systems such as Windows.
- 3- The pre-programmed functions in LabView FPGA VI can be integrated to build the code without spending time in writing text-based language for each function before using it.
- 4- With LabView FPGA module, the interface between the FPGA VI software and FPGA target is fast comparing with other traditional programs.
- 5- LabView FPGA module makes simultaneous execution of parallel tasks, which reduces the execution time and makes Real-Time measurements possible.
- 6- Using the host interface for the FPGA VI can also reduce the executing time of the code and make it robust.

However, LabView FPGA model requires time to understand it and to use it efficiently. Working with LabView FPGA module needs the basic understanding of its main components and their functions.

3. 2 Principles of LabView FPGAs

LabView FPGAs are silicon chips with unconnected logic gates. The functionality of the FPGA hardware can be defined using software to configure the FPGA gates. FPGAs are used in applications that require reconfiguration in the field.

National Instrument LabView FPGA system contains two essential parts; these parts are LabView FPGA VI, which is a software running in Windows, and a reconfigurable input/output (RIO) hardware or FPGA target. Intermediate files and bit files do the

interfacing between LabView FPGA VI and FPGA target during compiling as shown in Figure 3-1.



Figure 3-1. The interfacing between the software and hardware devices.

This process takes time to change the intermediate files that carry the build-code in LabView FPGA VI to a bit file in compile service and send it back to FPGA VI. The interfacing is done by pressing the “run” button on the FPGA VI after building the program. This can save valuable time for users instead of spending a long time to learn low level design tools for doing a measurement.

3.3 LabView FPGA-based measurement system

The LabView FPGA measurement system is based on the four following principles;

- 1- LabView software is running in Windows.
- 2- National Instrument Reconfigurable Input Output (NI-RIO) is the driver software that is used to interface between LabView software and hardware devices as shown in Figure 3-2.
- 3- LabView FPGA hardware allows users to use software to define the functionality of hardware devices.
- 4- Reconfigurable I/O hardware or (R series DAQ), is the data acquisition card that collects the real data from units under test and presents it on the computer.

Data acquisition card “PCI-7831R” is the card used in our measuring system to interface between LabView software and hardware devices as seen in Figure 3-2.

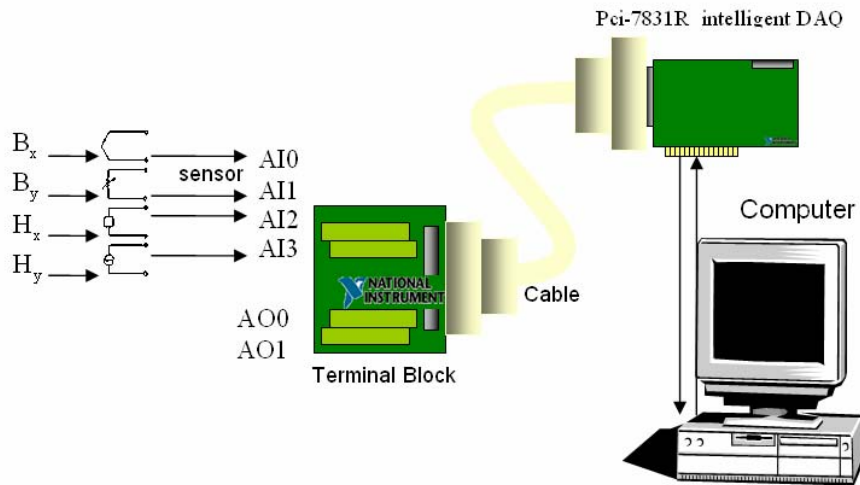


Figure 3-2. The interface between the real world applications and the computer through the NI PCI-7831R intelligent DAQ.

The data acquisition card is sampling the real functions in real applications to generate data that a computer can handle. Sometimes abbreviated DAQ or DAS, data acquisition typically involves acquisition of signals and waveforms and processing of the signals to obtain the desired information (Gadre 1998, pp 3-4).

The components of data acquisition systems include appropriate sensors that convert any measurement parameter to an electrical signal. The data acquisition card acquires the electrical signals and a computer displays them as shown in Figure 3-2. In these measurements, the flux density and field strength components B_x , B_y , H_x and H_y are the desired data to be measured by PCI-7831R card and controlled by LabView on the computer.

Chapter4: Experimental work

This chapter introduces a method for measuring the power losses in electrical steel sheets. The method consists of setup devices and LabView FPGA software.

The very basic concept of the method is that the setup device resembles an electrical induction device as the sheets are used to build the core of the induction device. The yokes resemble to the stator of an electrical motor, and the exciting coils that are wound around the center of the yokes resemble the exciting winding for the machine. The aim of building the setup device is to avoid the difficulties of measuring the data from the real device.

The LabView FPGA program is used to collect the flux density and magnetic field strength components and calculate the power losses. The complete description of the setup devices and the used LabView FPGA program follows.

4.1 Description of the measurement setup

Figure 4-1 shows a photograph of the measuring device used to measure the power losses in the electrical steel sheets.

The measuring device consists of two pairs of double U-shaped yokes. Each yoke is built of 520 items of thin electrical steel plates with thickness of 0.2 mm. A Polyester film material separates the items in order to reduce eddy currents. The thickness of the polyester film is 0.19 mm. The two pairs of U-shaped yokes are wound with 400 turns of exciting coils, which are set around the cores to magnetize them with the desired magnetic field. The arrangement of the exciting coils made it possible to subject high flux density through the yokes to the sample sheets.

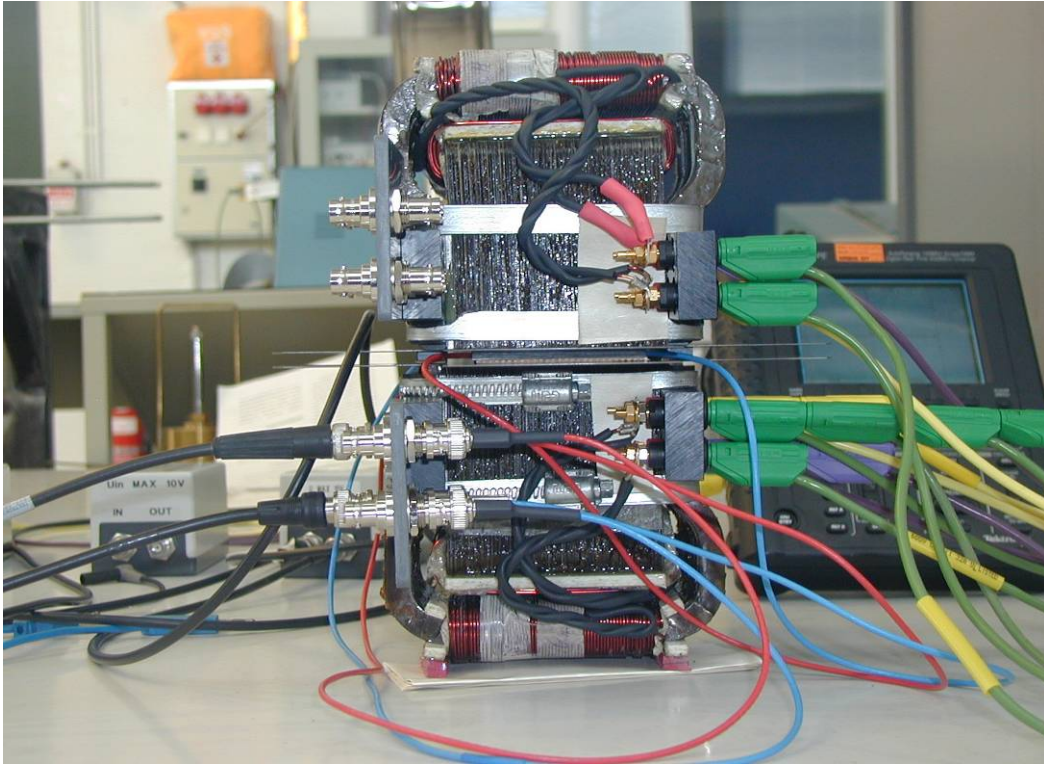


Figure 4-1. The construction of the measuring device.

Figure 4-2 shows one of the two electrical sheet samples used and its dimensions. There are four holes in the sample with a diameter of 1 mm for each one. The distance between each two holes in the same axis is 20 mm. Through each holes in the same direction, two turns of B-coils are wound around the sample, the B-coils are used to measure the flux density components, B_x and B_y in the area of over 400 mm². H-coils, consisting of 900 turn each are arranged tangentially to the sample to measure the magnetic field strength components.

In this method, B-coils and H-coils are connected to four terminals in a terminal block that is connected through a SH68-C-S cable to the NI PCI-7831R card. The NI PCI-7831R is used to complete the interfacing and to transfer the data between the measuring device and the LabView FPGA program. The description of the LabView FPGA program used is presented in details in Section 4.2.

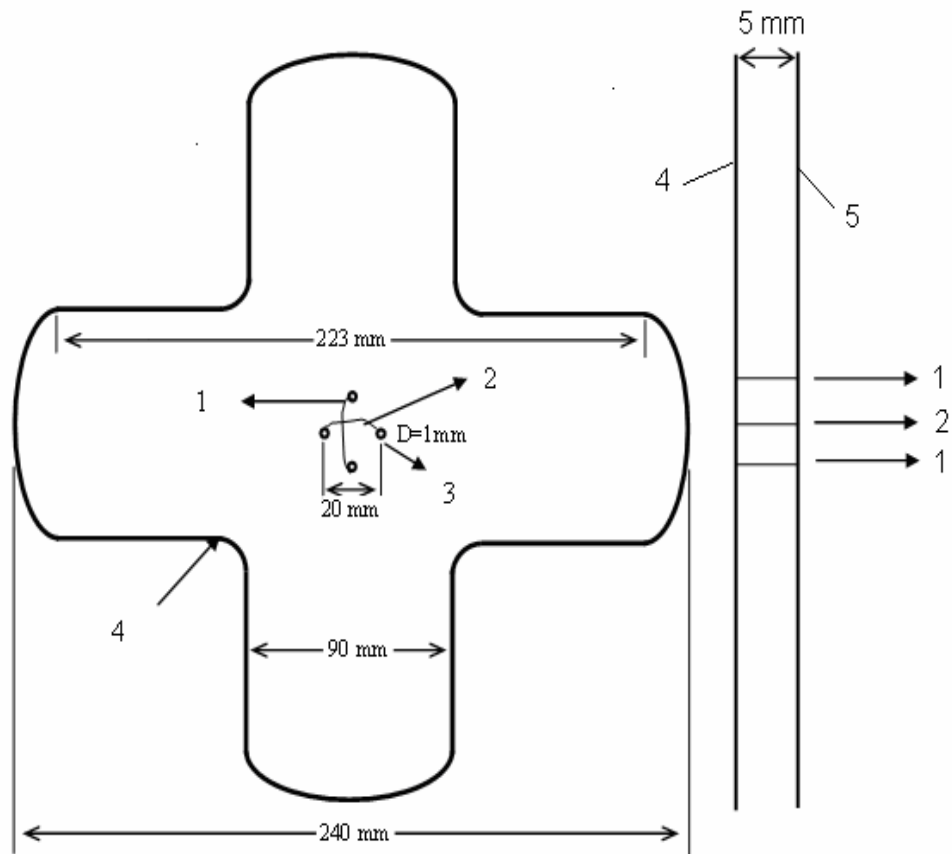


Figure 4-2. Dimensions of the electrical sheet sample and the construction of B-coils.

In Figure 4-2 we can see the following:

- 1- B-coils in x-direction.
- 2- B-coils in y-direction.
- 3- a drilled hole in the sheet with diameter of 1 mm.
- 4- the first electrical steel sheet.
- 5- the second electrical steel sheet.

Figure 4-3 shows a picture of the electrical steel sheets and the construction of B-coils. H-coils are in between the two sheets.

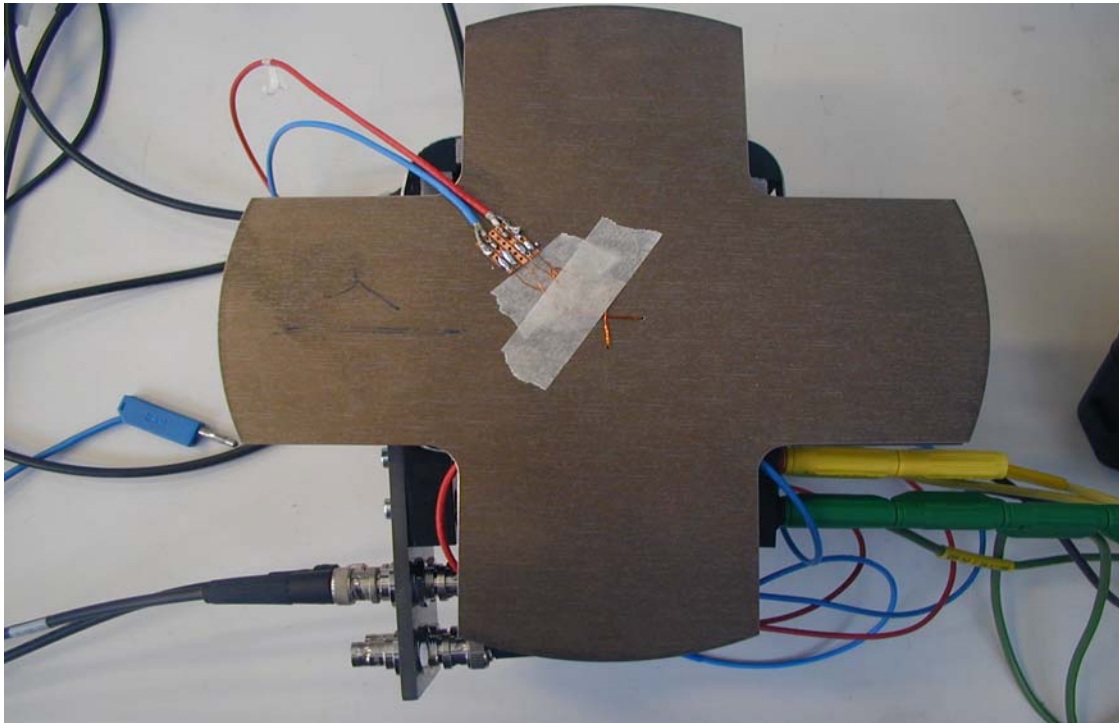


Figure 4-3. The construction of B-coils in the electrical steel sheets.

4.2 LabView FPGA program for measuring power rotational losses

In order to build the desired program with LabView FPGA module and to use it for measuring the power losses, some important steps have to be taken. They are presented as follow;

- 1- A new project in LabView FPGA module in the project explorer is opened.
- 2- FPGA target which is INSTR::PCI-7831R target from the computer is chosen by selecting the item detecting targets and devices.
- 3- The analog inputs and outputs from FPGA target are configured by selecting “new” and then an FPGA I/O item is selected where the desired FPGA I/Os are dragged to the project.
- 4- The other resources, that are necessary to build the program, are configured. They are; one onboard clock, First In First Out Direct Memory Access (DMA

FIFO), and then a special channel for the memory is defined with specific depth.

5- A new VI is opened where both Block Diagram and Front Panel are found to build the desired program.

6- The FPGA VI program is built by putting the needed functions on the Block Diagram and wiring them in a correct manner.

7- After completing the FPGA VI program, it is compiled to FPGA target.

8- The host VI is built in the same project explorer on the computer in order to add some functions that cannot be added on FPGA VI and also to make a robust code for the program.

After these steps, the program becomes ready to measure the rotational power losses in electrical steel sheets. The used program consists of two parts as previously mentioned. The first part that is built on FPGA target contains the Front Panel and the Block Diagram. Figure 4-4 shows this Block Diagram.

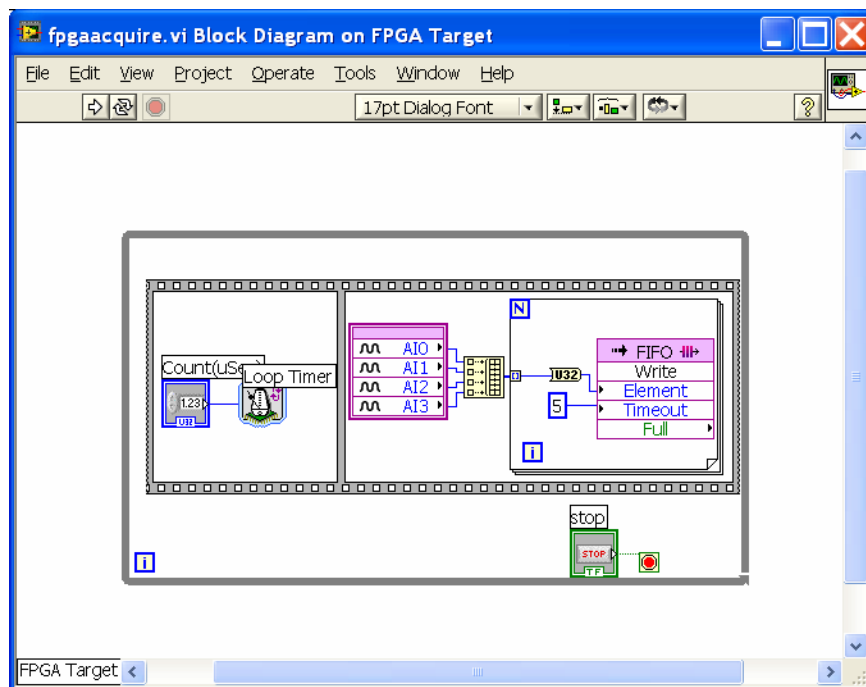


Figure 4-4. The Block Diagram of the program on FPGA target.

In the following, there is an explanation about all the used functions and how the program executes them.

First, there are four analog inputs: AI0, AI1, AI2, and AI3. They are used to receive the data of the flux density components B_x , B_y and the magnetic field strength components H_x , H_y from the measuring device. The data of the flux density and magnetic field strength components are passed directly to a build array to append them and send them through a “for” loop to the FIFO-Write to transfer it from the target to the host in sequential way. The FIFO memories on FPGA target and host work as one memory. Therefore, after compiling the program there is no need to run FPGA target to measure the data. The FPGA-program is actually called by the host program. Another step before transferring the data from the target to the host is to convert the data to 32-bit unsigned integer as required by the DMA FIFO.

Figure 4-5 shows the second part of the used program, which is the host VI where the rest of the measurements are done.

In this part of the program, there is an open FPGA VI reference to open reference to the FPGA VI target and communicate between the host VI and the FPGA VI. The open FPGA reference is connected to FIFO-Configure to determine the depth of the memory on the host. Otherwise, the depth of the FIFO memory on the host will be twice its depth on FPGA target. There is also FIFO-Read to receive the stored data from FPGA target and write it to a text file through a number of conversions.

A program written in MATLAB software is used to analyze and plot the saved data. Finally, the losses are calculated from the saved data.

The total magnetic power losses in the sheets are computed as (Brix et al.1984).

$$P_{\text{tot}} = \frac{1}{T} \int_T \left(H_x \frac{dB_x}{dt} + H_y \frac{dB_y}{dt} \right) dt \quad \text{w/m}^3 \quad (8)$$

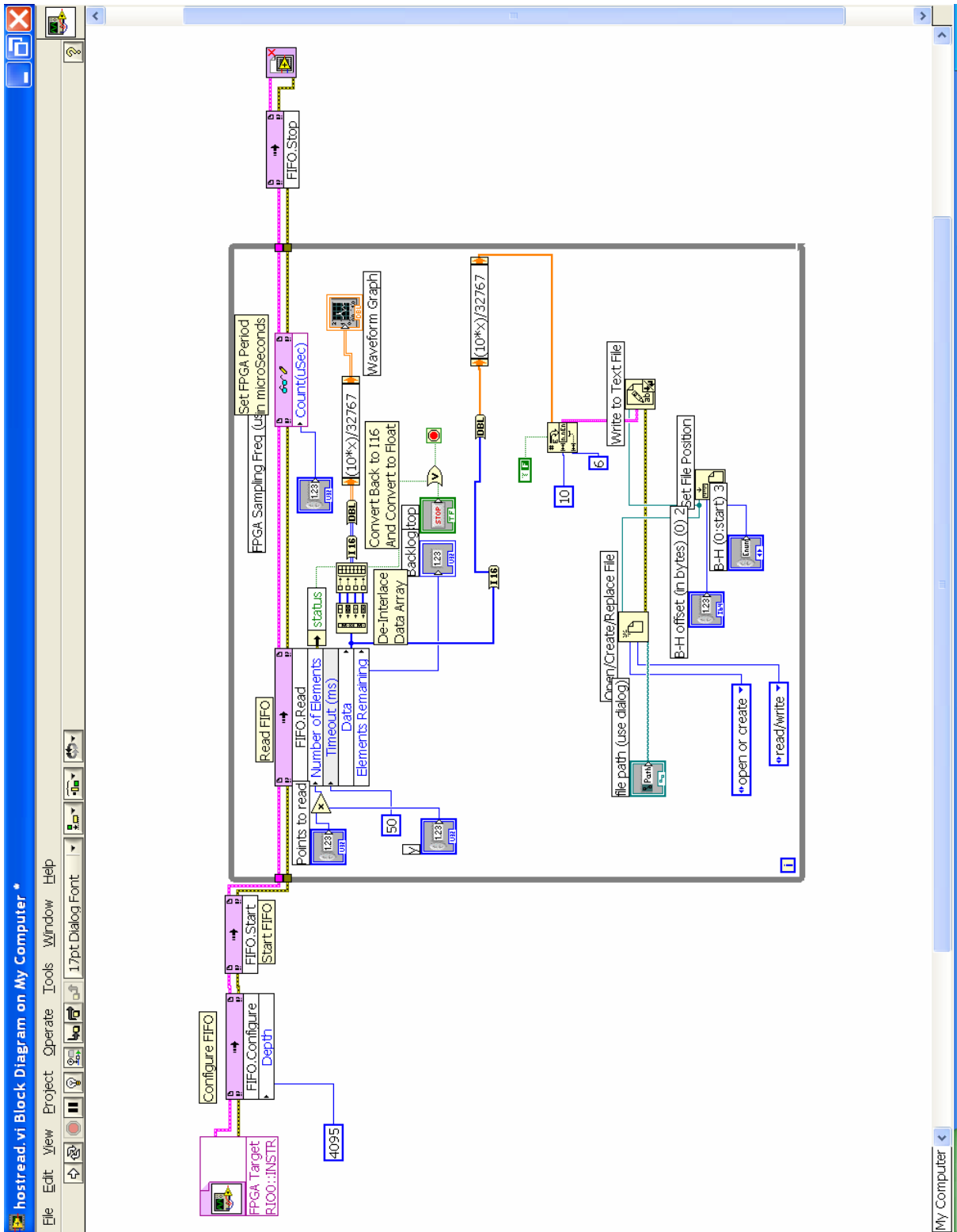


Figure 4-5. Block Diagram of the host VI.

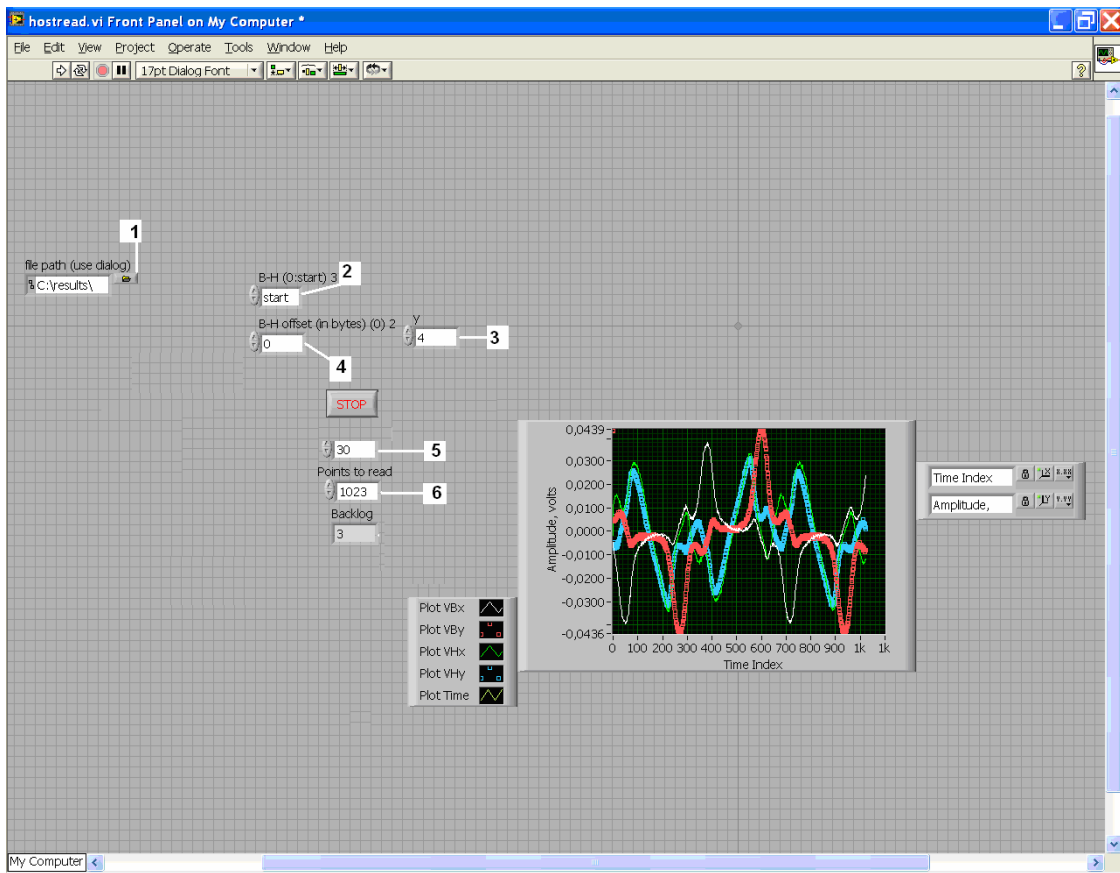


Figure 4-6. The Front Panel of the host VI.

Figure 4-6 shows the front panel of the host program. There are six controllers, which are;

- 1- the file path, where the data pass through it to the text file.
- 2- a control button used to chose the type of the data that can be save in the text file.
- 3- a control button used to determine the number of signals, which can be plotted.
- 4- a control button to change the offset of the signals.
- 5- the sampling time in μs .
- 6- the number of the elements for each signal.

On the left of the scope, there is the number of points or elements for each component that have been taken from the sample (1023 elements). Right above the points to read, there is the sampling time, in our case it was 30×10^{-6} seconds.

In Figure 4-7, there is a plot of the measured signals as function of time in 2D measurements.

1- B_x - signal.

2- B_y - signal.

3- H_x -signal.

4- H_y -signal.

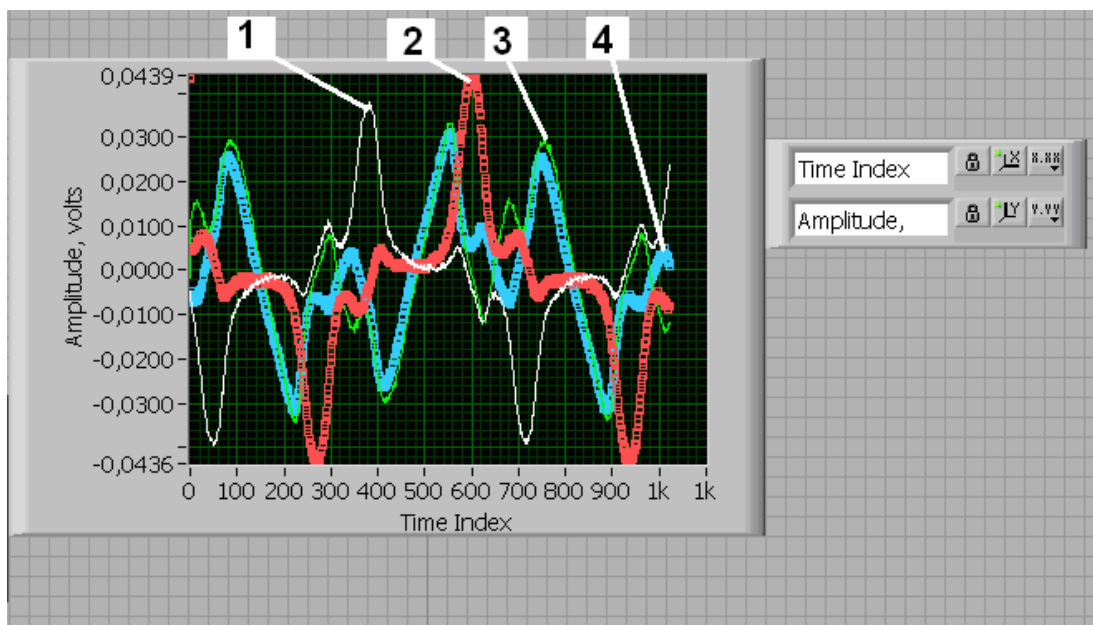


Figure 4-7. The waveforms of the measured signals.

5- Results

The DAQ (Data Acquisition) NI PCI-7831R and LabView FPGA module are used for acquiring the signals from the measurement device. In order to compute the flux density and magnetic field quantities, the difference in potential between the ends of the coils was acquired.

In this part of work, the power losses are calculated and plotted in different conditions. The influence of increasing the flux density on power losses is explained. The measurements were done under two different frequencies and several voltage excitations, the frequencies were 50 and 200 Hz. In each measurement, the flux density, magnetic field strength, remanence flux density and coercivity of the magnetic field were determined and arranged in a table that is presented in the last subsection.

5.1 1D measurements

a. Frequency of 50 Hz

Under low excitation field, i.e. low voltage (~ 2 V), Figure 5-1 shows the behavior of B_x - H_x curve in 1D- measurements. The magnetic flux density through the material is changing with the variation of the applied external field. This change behaves in such manner that is not linear due to the physical properties of the material. This is seen in Figure 5-2 and 5-3. The behavior of B_x is relatively sinusoidal but it is not purely. The non-linearity between B_x and H_x can be seen more clearly in the behavior of H_x compared with the behavior of B_x at the same time. In this measurement, the total power losses are 80 J/m^3 , the peak value of the flux density is 0.5 T and that of the magnetic field strength is 70 A/m .

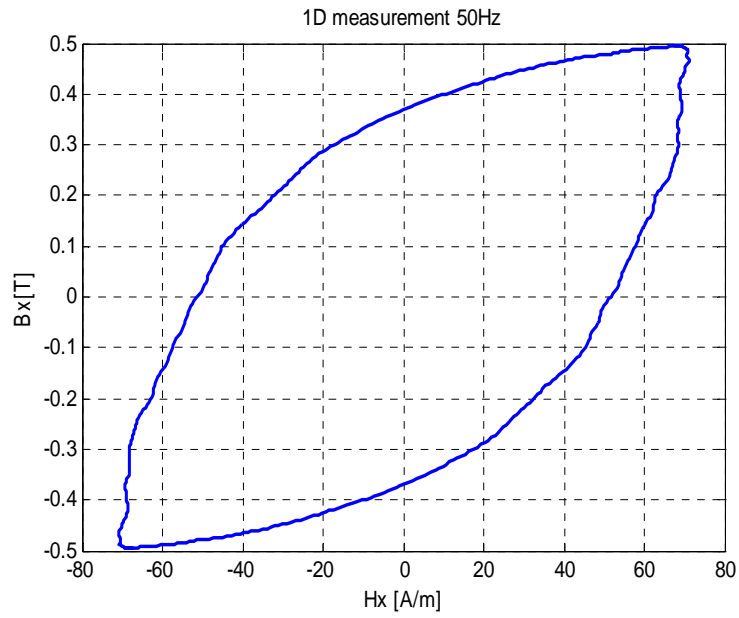


Figure 5-1 The relation between H_x and B_x at 50 Hz, $\hat{B}_x = 0.5$ T.

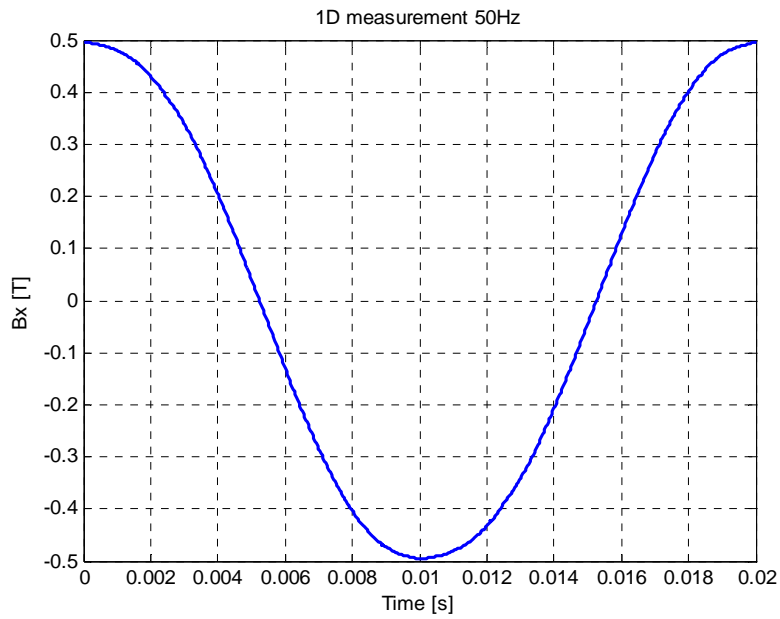


Figure 5-2 The instantaneous value of B_x at 50 Hz, $\hat{B}_x = 0.5$ T.

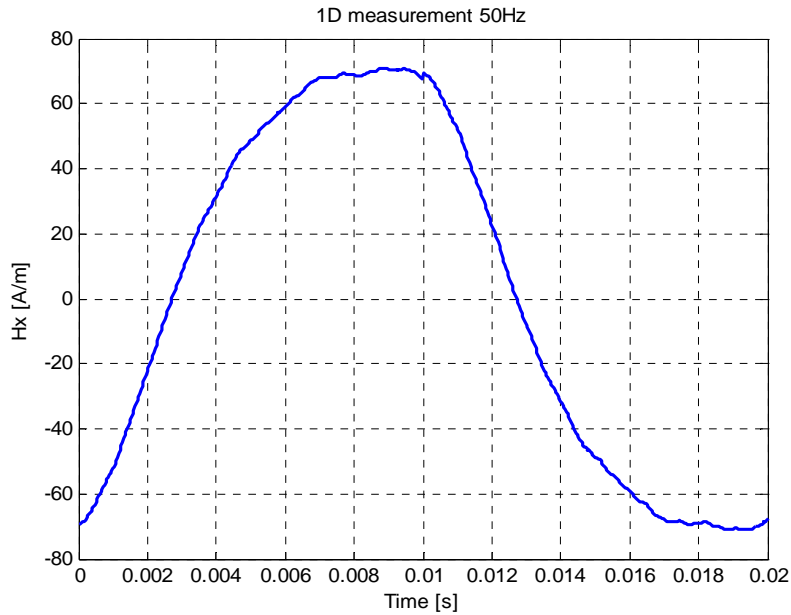


Figure 5-3 The instantaneous value of H_x at 50 Hz, $\hat{H}_x = 70$ A/m.

With the increase of the external applied field, the flux density increases in the electrical steel sheets as shown in Figure 5-4, that leads to an increase in the loop area and increase of the power losses (220.4 J/m^3). The behavior of B_x and H_x has an impact on the increase of the power losses shown in Figure 5-5 and Figure 5-6.

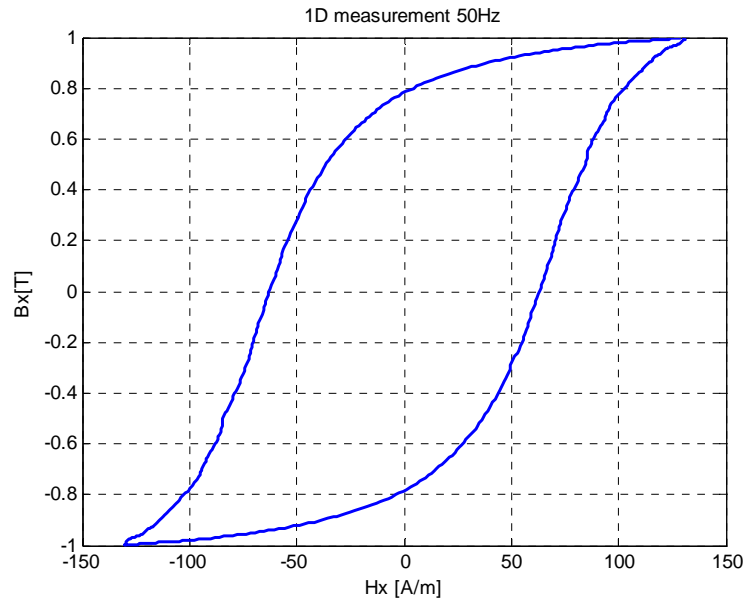


Figure 5-4 The relation between H_x and B_x at 50 Hz, $\hat{B}_x = 1$ T.

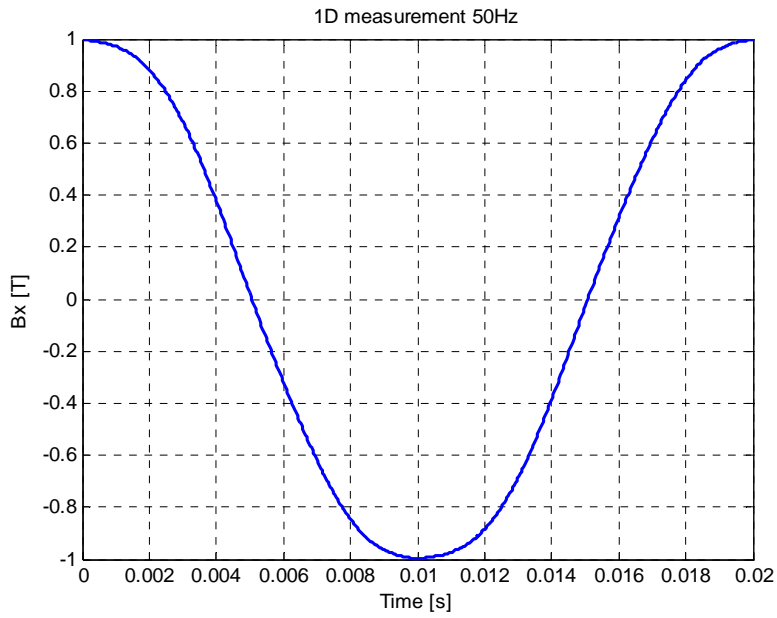


Figure 5-5 The instantaneous value of B_x at 50 Hz, $\hat{B}_x = 1$ T.

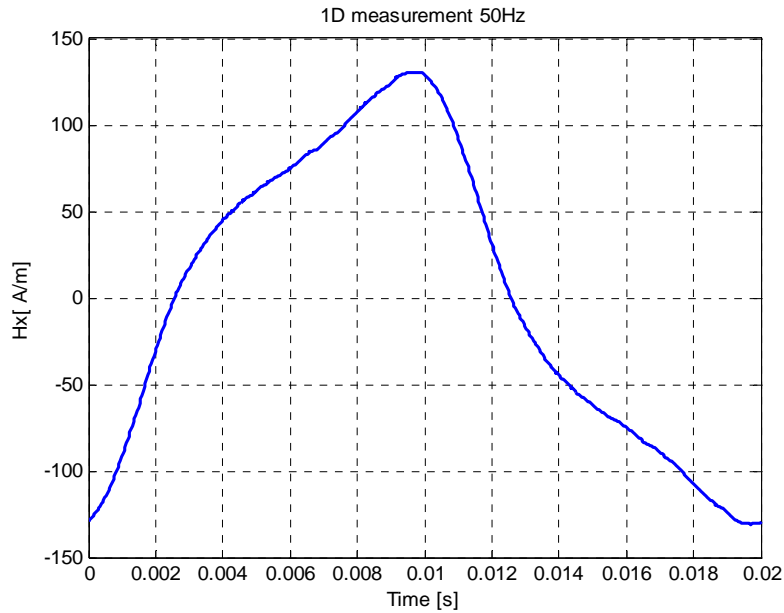


Figure 5-6 The instantaneous value of H_x at 50 Hz, $\hat{H}_x = 130.7$ A/m.

As the external applied field increases, the flux density and magnetic field strength increase as seen in Figure 5-7. The maximum value of the flux density is 1.5 T and the magnetic field strength is 1200 A/m. Under high excitation field, the increase of B_x becomes more slowly comparing with the increase of H_x . The total power losses of this measurement are 665 J/m^3 . They have increased three times compared with those at flux density 1 T. Due to this increase of the power losses, the non-linearity of the behavior of B_x and H_x became more obvious as shown in Figure 5-8 and in Figure 5-9.

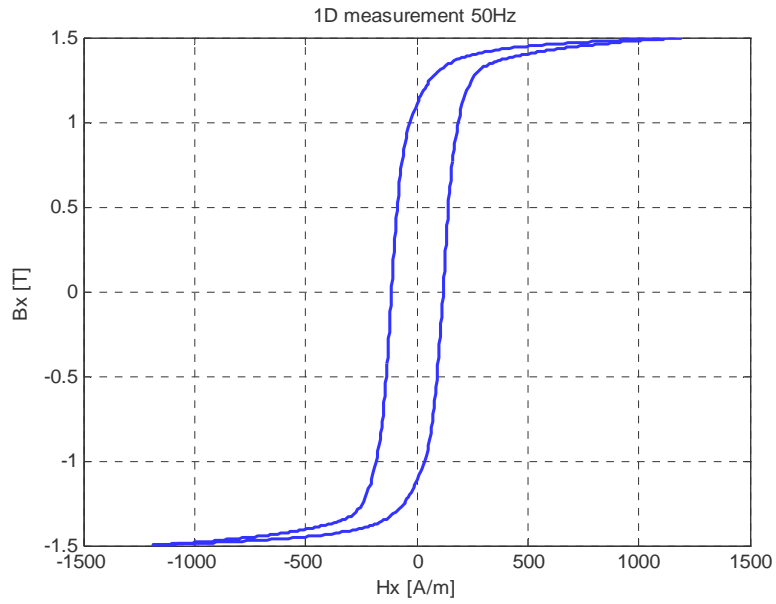


Figure 5-7. The relation between H_x and B_x at 50 Hz, $\hat{B}_x = 1.5$ T.

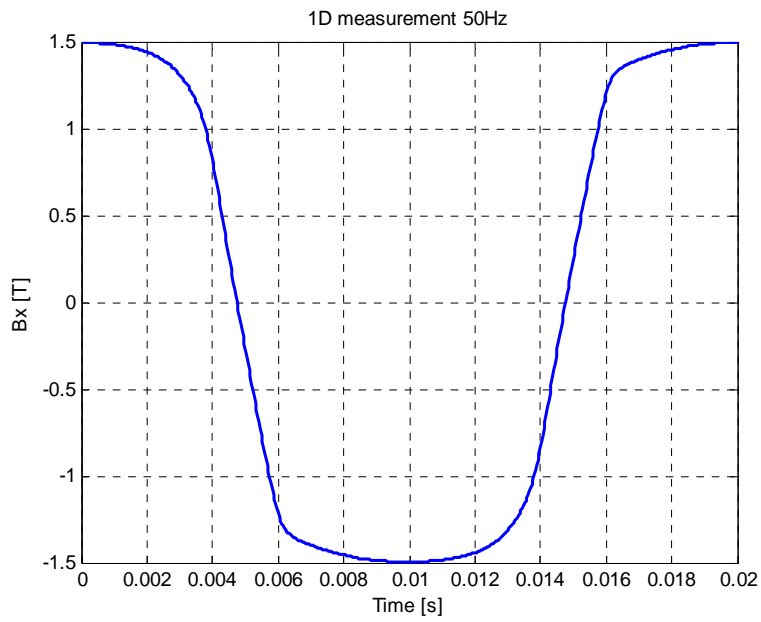


Figure 5-8. The instantaneous value of B_x at 50 Hz, $\hat{B}_x = 1.5$ T.

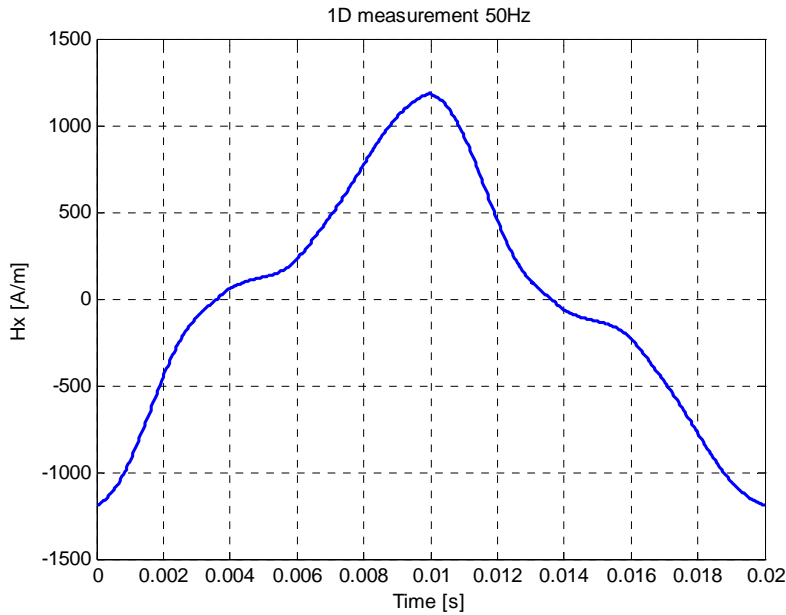


Figure 5-9 The instantaneous value of H_x at 50 Hz, $\hat{H}_x = 1200$ A/m.

When we applied the external field in y-direction, there were some differences in the area of the loops, and in coercive magnetic field strength, i.e. in the power losses. There is a difference in the power losses depending on the direction of magnetization for the same amplitude of the magnetic flux density. Figure 5-10 presents the difference in the area of the loop at the same value of the flux density compared with the x-direction presented in Figure 5-7. The cause of that difference goes to the anisotropy of the material. In this measurement, the maximum flux density was also 1.5 T but the maximum magnetic field strength and the total losses were only 930 A/m and 460 J/m^3 , about 30% less in y direction than in x direction. For the same reasons that have been mentioned previously, the shape of the flux density component B_y is not sinusoidal as shown in Figure 5-11. The behavior of the magnetic field strength component H_y is more complicated as shown in Figure 5-12.

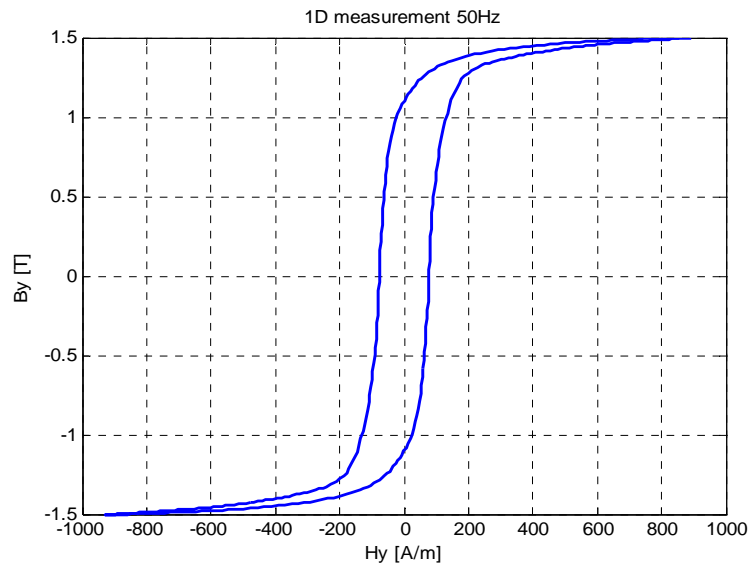


Figure 5-10. Y-direction measurement at 50 Hz, $\hat{B}_y = 1.5$ T.

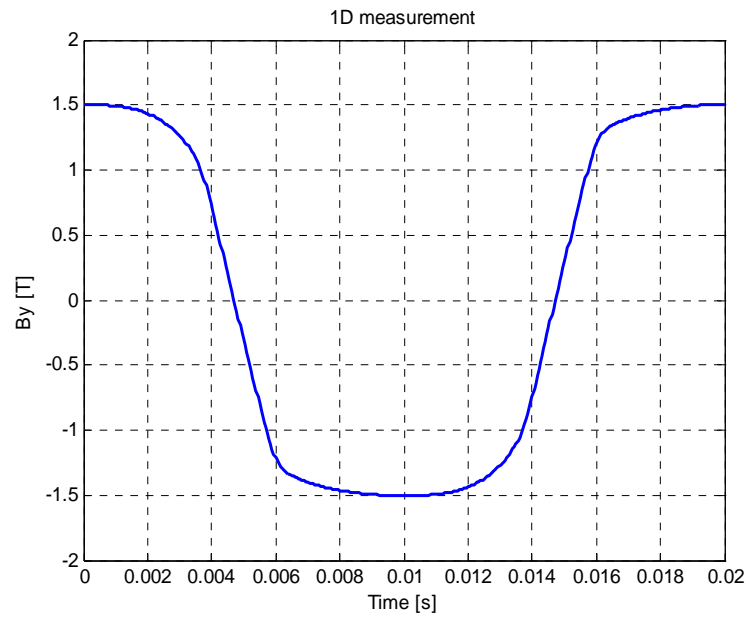


Figure 5-11. The instantaneous value of B_y at 50 Hz, $\hat{B}_y = 1.5$ T.

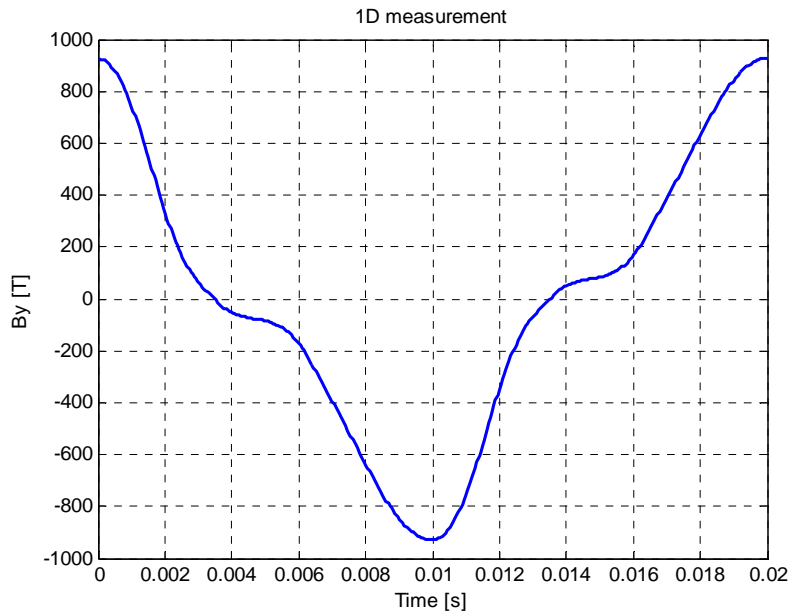


Figure 5-12. The instantaneous value of H_x at 50 Hz, $\hat{H}_x = 925$ A/m.

Figure 5-13 shows the effect of the flux density \hat{B}_x on the power losses in one-directional measurements. Under low excitation field, the measured \hat{B}_x was 0.5 T and the total power losses were 80.9 J/m^3 . As the excitation field increases, the flux density component increases and the power losses increase. They reach 220.4 J/m^3 when \hat{B}_x is 1 T. The increase of the power losses with the increasing of \hat{B}_x is still valid when \hat{B}_x reaches 1.5 T.

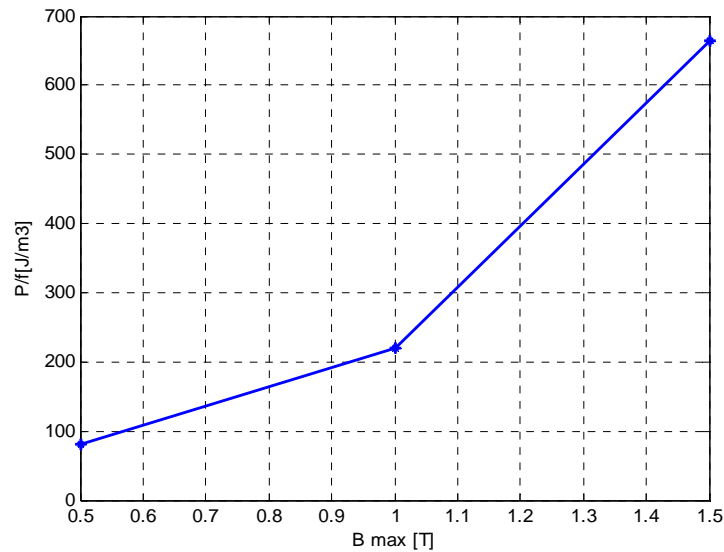


Figure 5-13. The relation between \hat{B} and the power losses at 50 Hz.

b. Frequency of 200 Hz

In the next measurements, the frequency has been increased to 200 Hz. The maximum flux density is a little higher than 1 T in Figure 5-14. In Figure 5-13, the total power losses at the same flux density and frequency are about 220.4 J/m³ but in this measurement, they increased to about 384.9 J/m³. The increase of the power losses is due to the increase of the frequency.

In Figure 5-15 when \hat{B}_x reaches 1.5 T at 200 Hz, the power losses are still increasing, they are about 850.8 J/m³, which is 2.2 times higher than those at 1 T and 200 Hz and 1.27 higher than those at 1.5 T and 50 Hz.

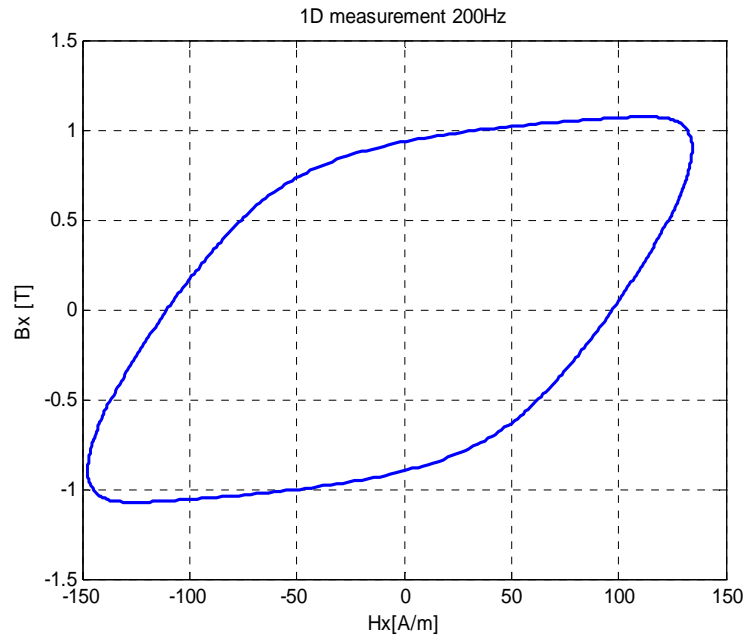


Figure 5-14. The relation between H_x and B_x at 200 Hz and 1 T.

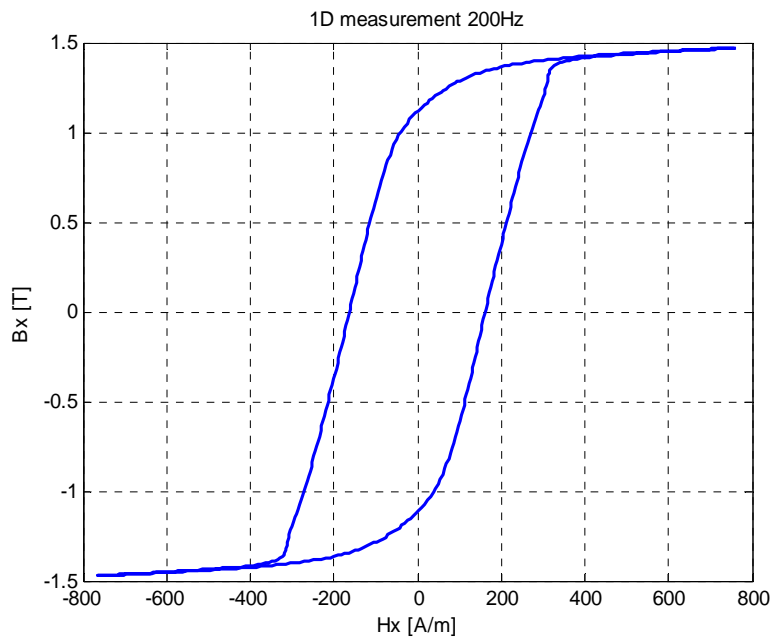


Figure 5-15. The relation between H_x and B_x at 200 Hz and 1.5 T.

5.2 2D measurements

a. Frequency of 50 Hz

This part of work is related to 2D measurements. We applied the same principle that we did in one-direction measurements, but this time the excitation was in two-directions.

First, we input low values of sinusoidal voltage in both directions in the exciting coils, their peak values were approximately 2 V and the phase angle between them was 240° . Figure 5-16 presents the obtained B-H loops in both directions. The maximum flux densities of this measurement are 0.31 T in x-direction and 0.36 T in y-direction. Without using control, it is quite complicated, for instance, to get circular or elliptical shape of the loci of the flux density. Therefore, the loci of the flux density and magnetic field strength are not predictable as shown in Figure 5-17 and Figure 5-18.

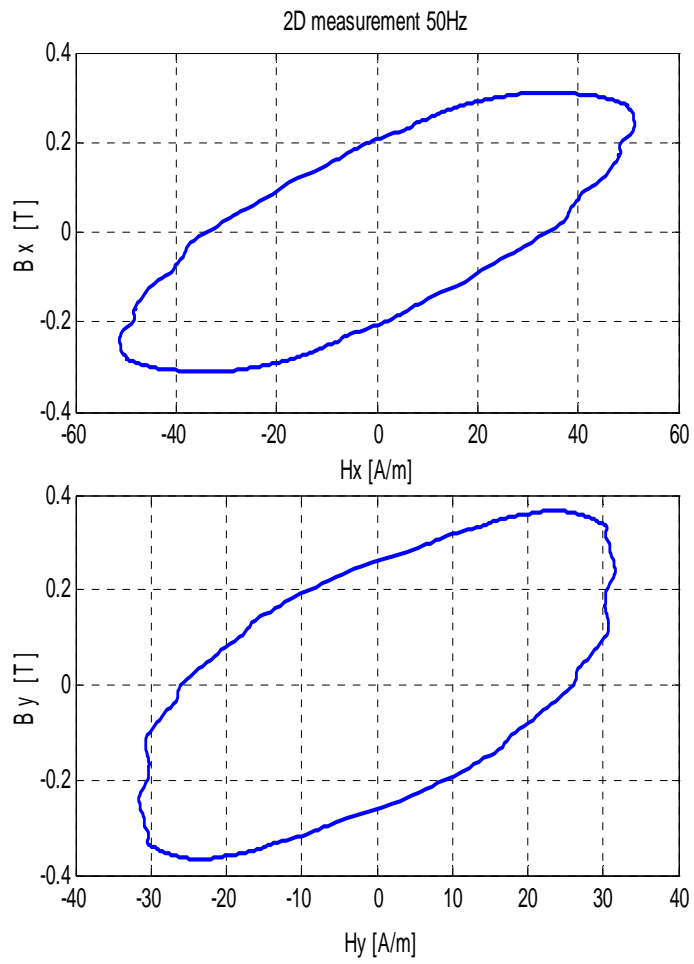


Figure 5-16. B-H loops in two-direction measurements at 50 Hz, $\hat{B}_x=0.31$ T and $\hat{B}_y=0.36$ T.

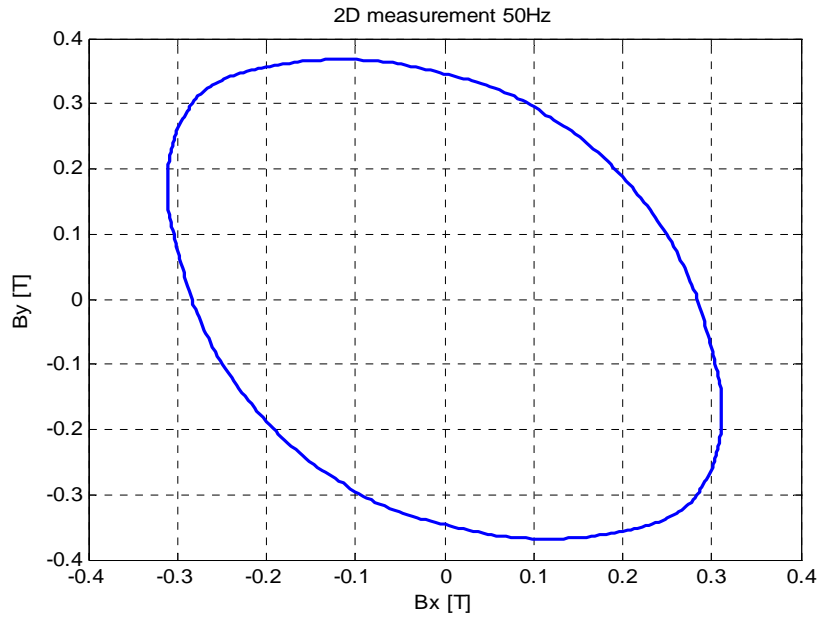


Figure 5-17. Loci of the flux density at 50 Hz $\hat{B}_x = 0.31$ T and $\hat{B}_y = 0.36$ T.

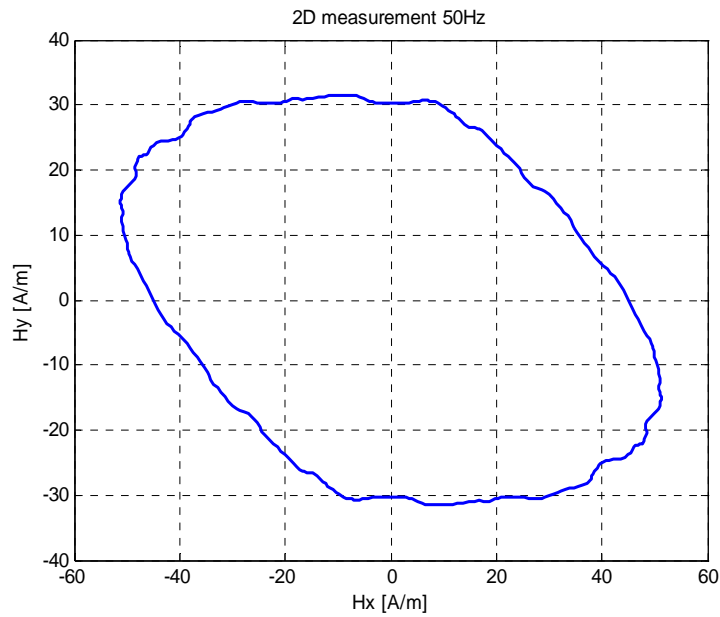


Figure 5-18. Loci of magnetic field strength at 50 Hz, $\hat{H}_x = 51.2$ A/m and $\hat{H}_y = 31.5$ A/m.

Figure 5-19 shows the behavior of B-H loops after increasing the excitation voltage to 15 V. The maximum of the magnetic flux density achieved is 0.9 T. There is a

difference in the behavior in x and y direction due to the next reasons. The material is anisotropic; the position of the electrical steel sheets is not exactly in the center of the yokes and, the flux density components are not controlled, in other words, they are not equal. In addition, the surrounding noise is responsible for some errors. The power losses are 4.6 times higher than those at 0.35 T. With the increase of the excitation voltage, the loci of the flux density and magnetic field strength as shown in Figure 5-20 and Figure 5-21 become different from those at low excitation (~ 2 v). The difference can be attributed to the anisotropy of the used material and to the arrangement of the domains during the excitation. This can be also seen in the rest of the loci's (Figures 5-23, 5-24, 5-26, and 5-27).

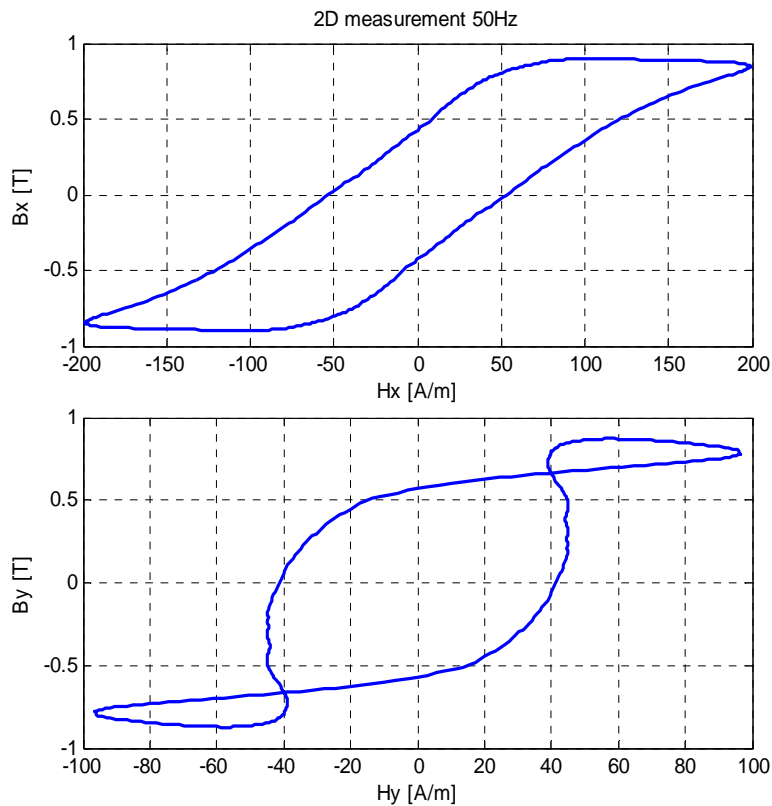


Figure 5-19. B-H loops in two-direction measurements at 0.9 T and 50 Hz.

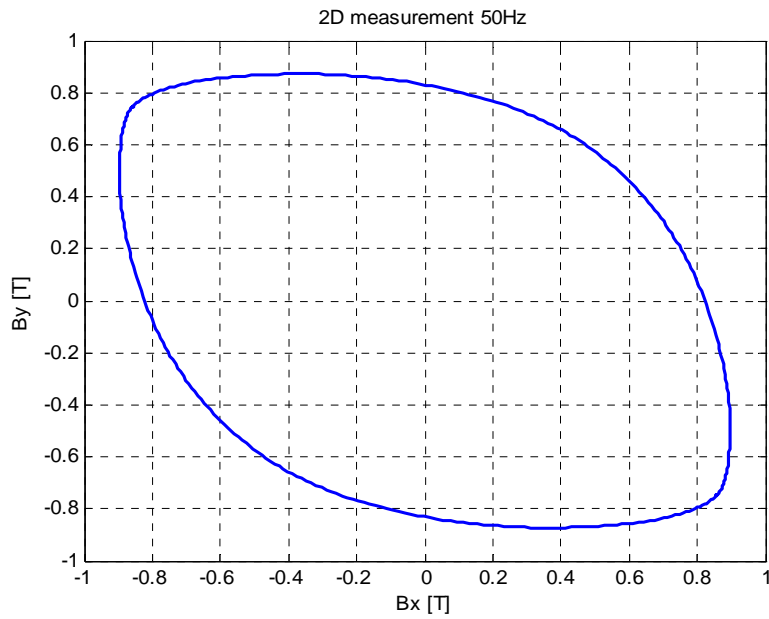


Figure 5-20. Loci of the flux density at 50 Hz, $\hat{B}_x = 0.89$ T and $\hat{B}_y = 0.87$ T.

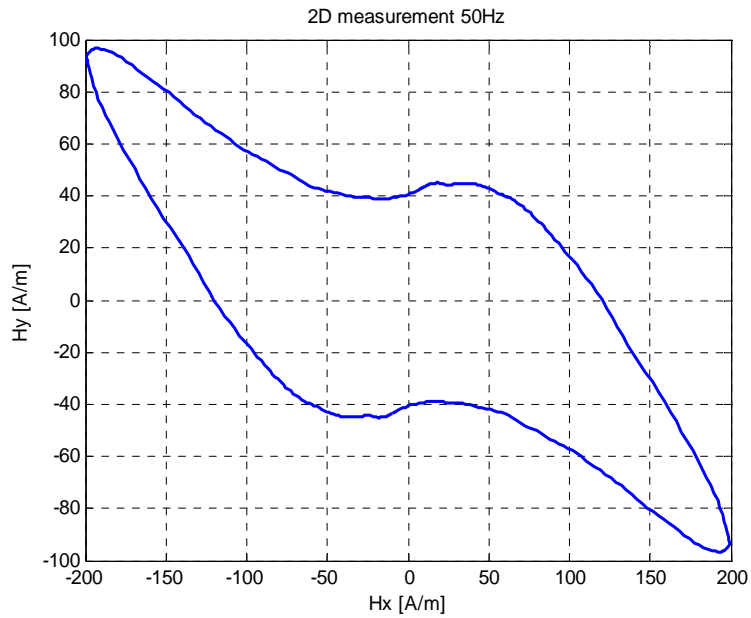


Figure 5-21. Loci of magnetic field strength at 50 Hz, $\hat{H}_x = 199$ A/m and $\hat{H}_y = 96.5$ A/m.

Figure 5-22 presents the shape of the B-H loops. In this measurement, the maximum flux density components are about 1.5 T in both directions. The maximum magnetic field strength component H_x is 0.1 bigger than the maximum magnetic field component H_y . The power losses are about 22.9 times higher than those at 0.35 T.

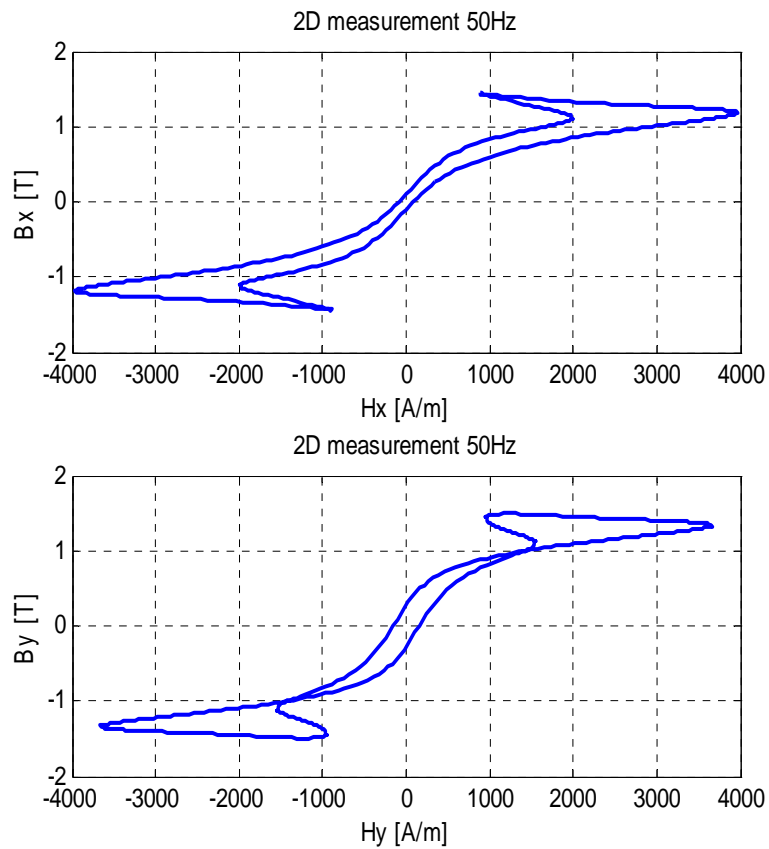


Figure 5-22. B-H loops in two-direction measurements at 1.5 T and 50 Hz.

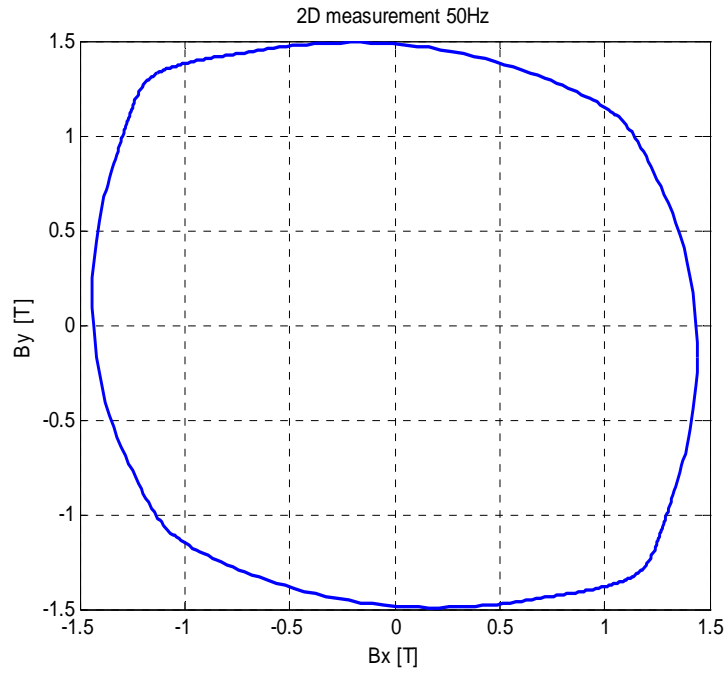


Figure 5-23. Loci of the flux density at 50 Hz, $\hat{B}_x = 1.44$ T and $\hat{B}_y = 1.5$ T

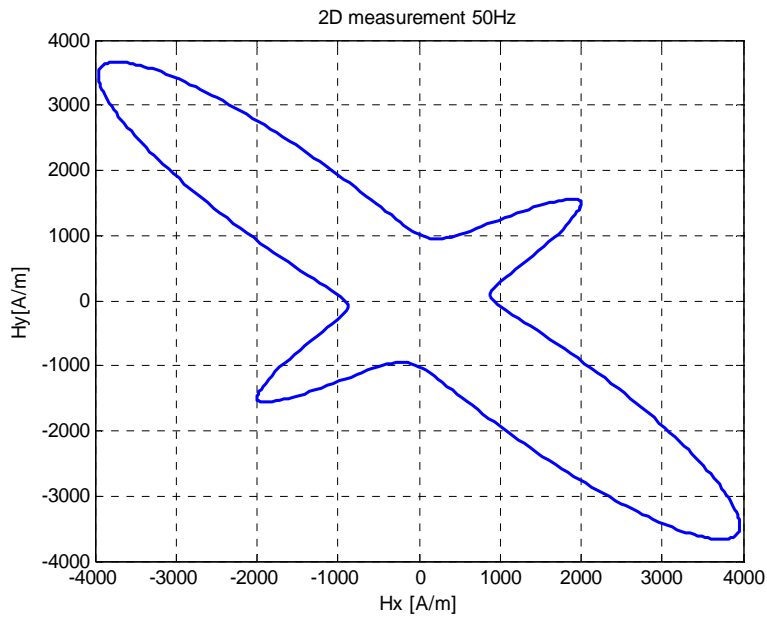


Figure 5-24. Loci of the magnetic field strength at 50 Hz, $\hat{H}_x = 3960$ A/m and $\hat{H}_y = 3670$ A/m.

In 2D measurements, the maximum flux densities are much higher than those at 1D measurements. They are 1.72 T in x-direction and 1.85 T in y-direction as shown in Figure 5-25. The difference of the maximum values of the flux density components may be caused by the design of the yokes. The magnetic field strength components are 11300 A/m in x-direction and 11250 A/m in y-direction. The power losses are increased to 1750 J/m³.

Figure 5-26 presents the loci of the flux density components B_x , and B_y . Their shape is not circular due to the uncontrolled excitation conditions. Figure 5-27 shows the loci of the magnetic field strength. The flux density and the magnetic field strength components are at the maximum values. Therefore, for any small changes in the flux densities, there is a big change in the magnetic field strength components.

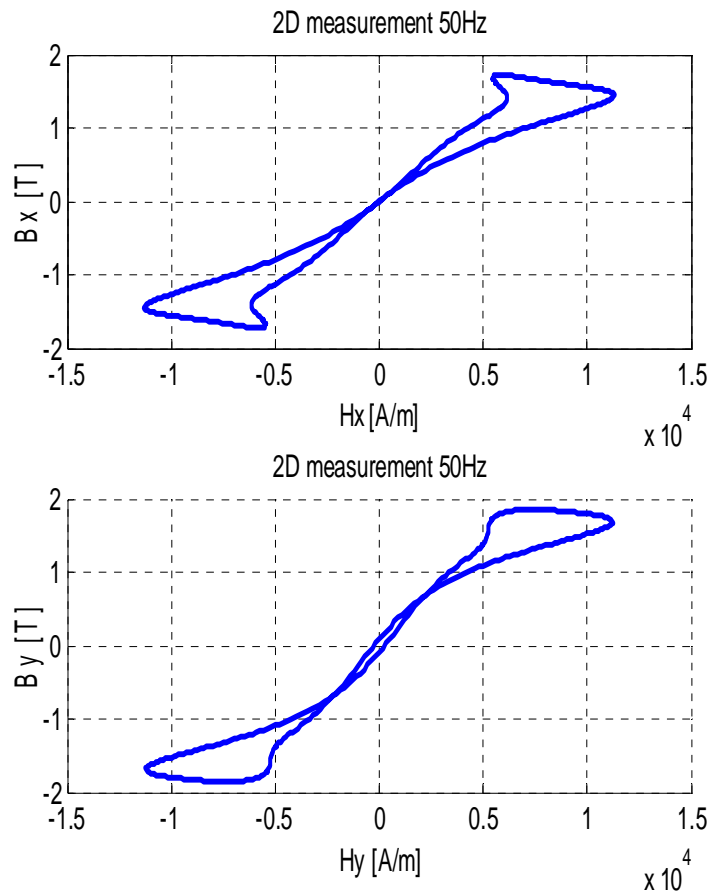


Figure 5-25. B-H loops in two-direction measurements at 1.72 T and 50 Hz.

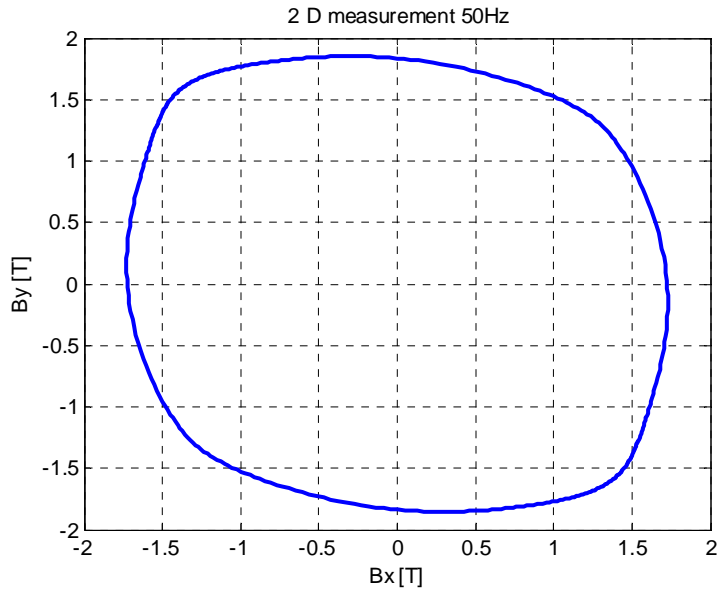


Figure 5-26. Loci of flux density at 50 Hz, $\hat{B}_x = 1.72$ T and $\hat{B}_y = 1.85$ T.

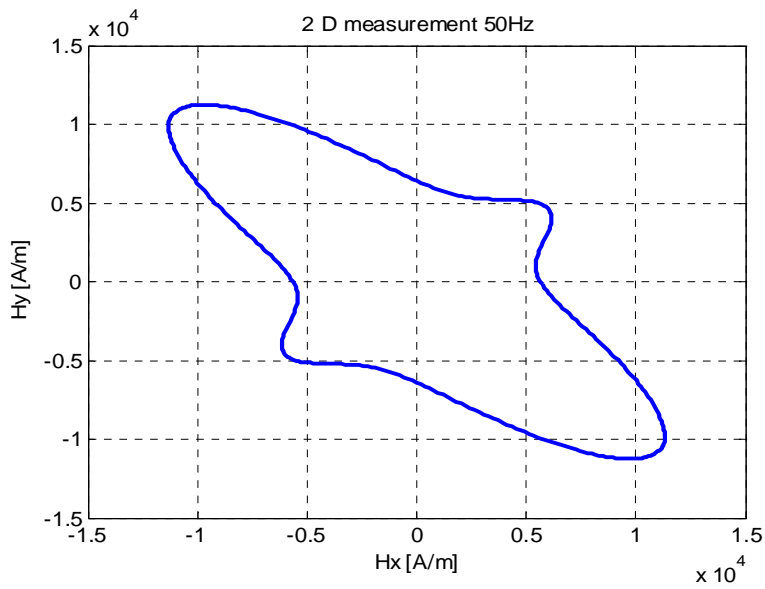


Figure 5-27. Loci of the magnetic field strength at 50 Hz, $\hat{H}_x = 11300$ A/m

and $\hat{H}_y = 11250$ A/m.

Figure 5-28 shows the effect of the flux density on the power losses in two-direction measurements. When the flux density is less than 1 T, the power losses are small (about 254.1 J/m³). After \hat{B} reaches 1T, the power losses are increasing largely. The maximum value of the power losses is at 1.7 T. By increasing \hat{B} to 1.72 T, the power losses decrease rapidly.

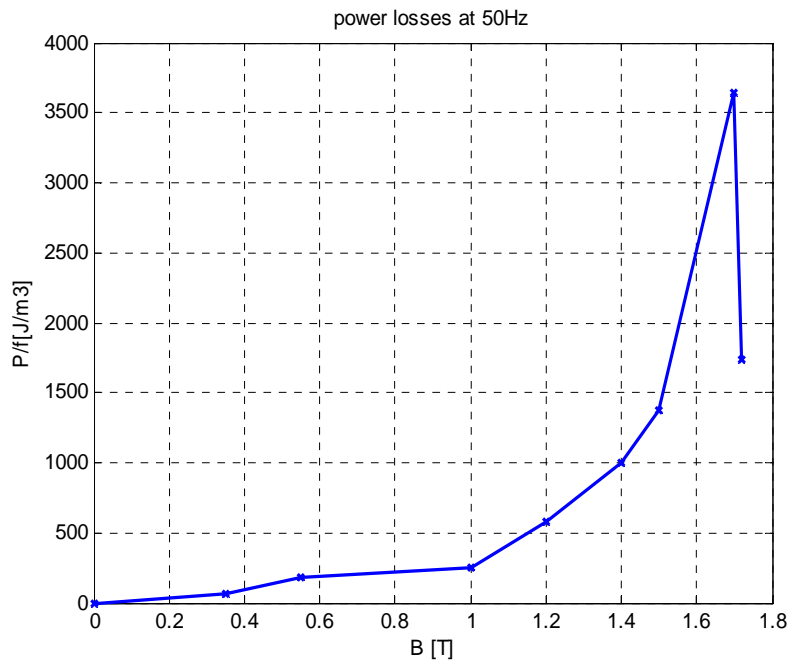


Figure 5-28. The effect of increasing \hat{B} on the power losses.

b. Frequency of 200 Hz

By increasing the frequency to 200 Hz, the excitation voltages have to be increased to reach the same flux densities of 1 T compared to the previous measurements done for 50 Hz. Due to the excitation conditions, the power losses are 1.9 times higher compared to those at 50 Hz and 1 T.

Figure 5-29 presents B-H loops at 200 Hz and 1 T. The behavior of the B-H loops is similar to the B-H loops at 1 T and 50 Hz.

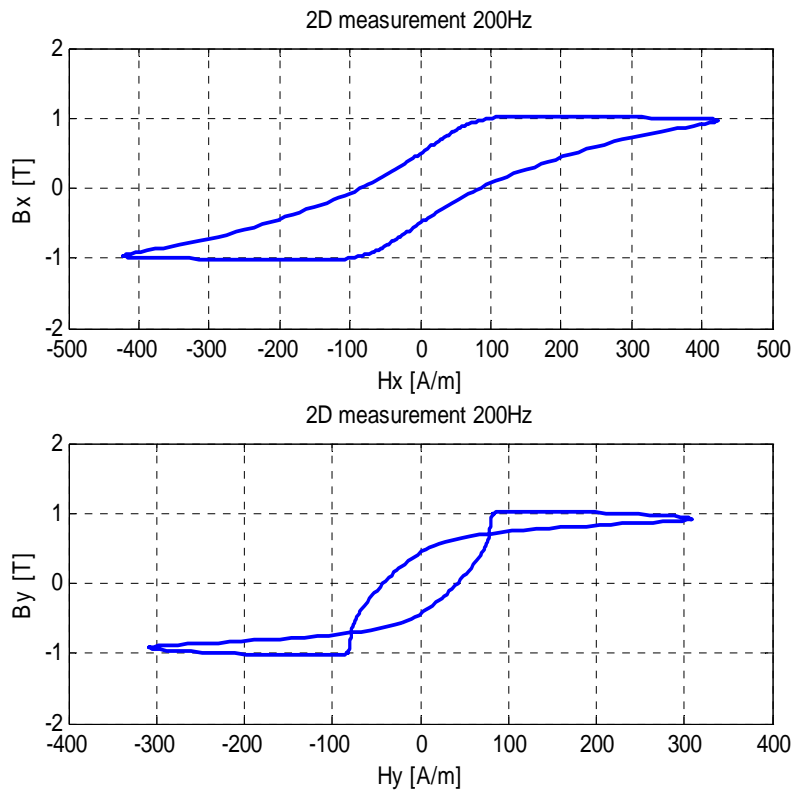


Figure 5-29. Loops at 200 Hz and $\hat{B} = 1$ T.

5.3 Summary Table of the results

Finally, the results for all measurements were arranged in one table. They are discussed in Section 6.

Table 1. Summary of the results.

Measurement	α_{ex}	B_{max} [T]	H_{max} [A/m]	f [Hz]	B_r [T]	H_c [A/m]	P_{tot} [J/m ³]
1	1D _x	0,5	71	50	0,37	51,6	80,9
2	1D _x	1	130,7	50	0,8	63,1	220,4
3	1D _x	1,5	1192	50	1,1	119,4	665,2
4	1D _y	1,5	929	50	1,1	77	460,2
5	1D _x	1	134	200	0,93	97,2	384,9
6	1D _x	1,47	762	200	1,12	161,5	850,7
7	2D	0,31	51,2	50	0,2	34	60,1
8	2D	0,9	199	50	0,42	53,4	277,7
9	2D	1,44	3960	50	0,1	80,9	1376,3
10	2D	1,7	8000	50	0,04	116	3436
11	2D	1,72	11320	50	0,007	31,2	1739,4
12	2D	1	420	200	0,5	83,5	486

α_{ex} is the direction of the excitation.

6. Conclusion

6.1 Discussion of the results

Under 1D excitation, the results have shown the behavior of $B_x - H_x$ loops in the electrical steel sheets. In these measurements, the range of the flux density, which has been used, started from 0.5 T and ended at 1.5 T. Due to the measurement device design, the maximum value of flux density was 1.5 T. Therefore, it was difficult to go higher than that point.

In this measurement, the minimum value of the magnetic field strength in x direction was 71 A/m and the maximum value was 1192 A/m. The results have shown the power losses and their relation with the flux density component B_x . The obvious increase of the power losses comes after the flux density B_x goes beyond 1 T. Although the flux density B_x reached high values, the power losses did not stop increasing.

The effect of the frequency on the power losses is now discussed. In the 50 Hz measurements at 1 T, the calculated power losses were 220.4 J/m^3 . In order to reach the same flux density of 1 T, higher excitation voltage was needed. The coercive field was about 63 A/m at 50 Hz and increased by 1.54 times at 200 Hz. However, there were no remarkable changes in the maximum magnetic field strength and the remanent flux density in both measurements as shown in Table 1.

In the two-direction measurements, the measurements have shown the power losses under different excitation conditions. Under low flux density, 0.35 T $B_x - H_x$ and $B_y - H_y$ loops were having almost the same shapes. By increasing the excitation voltage to about 15 V, the behavior of the two loops changed. This behavior was clear at the measured flux density 0.9 T, particularly in $B_y - H_y$. This change might be caused by the reasons that have been mentioned in the previous chapter. One thing to mention is that the flux density was increasing at some points even if the magnetic field was

decreasing, this kind of behavior has been early observed (Enokizono et al. 1990). In 2D measurements at 50 Hz, the maximum value of the flux density was 1.85T in y-direction and 1.72T in x-direction, the reason for this difference may be due to the excitation conditions and the anisotropy of the steel sheets.

6.2 Measurement setup

In all measurements, the data was acquired from the hardware devices using the NI card PCI-7831R and LabView FPGA module. During the measurements, some problems raised using this card. It was sensitive to the noise; the memory size limits the size and the time execution of the built program; using more memory for transferring the data from the FPGA VI to the host VI caused time delay even though the memories were connected in parallel. The host VI was an essential part of the used program and that took time to learn the interfacing between the two parts of the program. However, the card was reading the signals quite fast and accurately, the card was tested by generating signals from the generator and reading them by the card, it read exactly the same generated signals. Also, it was able to read high frequency signals up to 1000 Hz.

The other essential part of the measurement setup was the yokes. They were quite stable during the excitation. They could induce high field values in the electrical steel sheets, which reached about 1.85T in y direction. They worked quite nicely up to 400 Hz and the frequency can be increased further as well as there was no need for cooling the coils. However, some small problems were raised during the measurements: first, when we increase the excitation, some noise was heard and second, B-coils had to be changed many times during the measurements due to the broken isolation problem.

6.3 Importance of the work and suggestions

The results have shown the behavior of the power losses of electrical steel sheets under the 1D and 2D magnetic fields excitations . The results have shown the well-known hysteresis loop under 1D excitation field. The used material can be excited with high values of the magnetic flux density up to 1.85 T in y-direction and 1.72 T in x-direction and with high frequencies (up to 200 Hz). The behavior of B-H loops in the used material under different excitation fields has been presented. In addition, the results were reproducible.

For further work, the measurements should be done under controlled flux density.

7. References

Bertotti, G., 1998, Hysteresis in magnetism, Institute Electrotecnico Nazionale Calileo Ferraris, Torino Italy, AP academic press.

Boon, C. R., Thompson, J.E., 1965, "Alternating and Rotational Power Loss at 50c/s in 3% Silicon-Iron Sheet", *Proc. IEE*, Vol. 112, No. 11, November, pp 2147-2151.

Brix, W., Hempel, K. A., Schreder, W., 1982, "Method for the Measurement of Rotational Power Loss and Related Properties in Electrical Steel Sheets", *IEEE Transactions on Magnetics*, Vol. 18, No. 6, November, pp. 1496-1471.

Brix, W., Hempel, K. A., Schult, F. J., 1984, "Improved Method for the Investigation of the Rotational Magnetization Process in Electrical Steel Sheets", *IEEE Transactions on Magnetics*, Vol. 20, No. 5, September, pp. 1708-1710.

Chapman, S. J., 2005, Electrical Machinery Fundamentals, Fourth edition, Mc Graw Hill.

Enokizono, M., Suzuki, T., Sievert, J., Xu, J., 1990, "Rotational Power Loss of Silicon Steel Sheet", *IEEE Transactions on Magnetics*, Vol. 26, No. 5, September, pp. 2562-2564.

Enokizono, M., Tanabe, I., 1997, "Studies on a New Simplified Rotational loss Tester", *IEEE Transactions on Magnetics*, Vol. 33, No. 5, September, pp. 4020-4022.

Gadre, D., 1998, Programming the Parallel Port, R&D Books.

Goodenough, J. B., 2002, "Summary of Losses in Magnetic Materials", *IEEE Transactions on Magnetics*, Vol. 38, No. 5, September, pp. 3389-3408.

IEC Standard, Publication 404-2, Geneva: IEC Central Office 1978.

Ishihara, Y., Takahashi, N., 1979, Memoirs of the School of Engineering, Okayama University, Vol. 14.1, p. 15.

Ivanyi, A., Fuzi, J., Pfitzner, H., 1998, "2D/3D Models for a Three Phase Fed Single Sheet Tester", *IEEE Transactions on Magnetics*, Vol. 34, No. 5, September, pp. 3004-3007.

Kaplan, A., 1961, "Magnetic Core Losses Resulting from a Rotating Flux", *J. Appl. Phys*, Vol. 32, No. 3, March, pp. 370-371.

LabView User Manual, National Instruments Corporation, Austin Texas, April, 2003, pp.27-29.

Loises, G., Moses, A. J., 2001, "Critical Evaluation and Limitation of Localized Flux Density Measurements in Electrical Steels", *IEEE Transactions on Magnetics*, Vol. 37, No. 4, July, pp. 2755-2757.

Mori, K., Yanase, S., Okazaki, Y., Hashi, S., 2005, "2D Magnetic Rotational Loss of Electrical Steel at High Magnetic Flux Density", *IEEE Transactions on Magnetics*, Vol. 41, no. 10, October, pp. 3004-3007.

Moses, A. J., Thomas, B., Thompson, J. E., 1972, "Power Loss and Flux Density Distributions in the T-Joint of a Three Phase Transformer Core", *IEEE Transactions on Magnetics*, Vol. MAG -8, No. 4, December, pp. 3310-3312.

Del Toro, V., 1985, Electric Machines and Power Systems, Prentice-Hall, Inc., Englewood Cliffs, N.J. 07632, pp. 12-14.

Ramos, H. G., Girao, P. S., 1991, "A Rotating Field Automated Measurement System for the Characterization of Ferromagnetic Materials", *J. Appl. Phys*, Vol. 69, No. 6, April, pp. 5103-5105.

Reyne G., Meunier, G., Imhoff, J.F., Euxibie, E., 1988, "Magnetic Forces and Mechanical Behaviour of Ferromagnetic Materials", *IEEE Transactions on Magnetics*, Vol. 24, No. 1, January, pp. 234-237.

Sievert, J., 1990, "Recent Advances in the One- and Two-Dimensional Magnetic Measurement Technique for Electrical Sheet Steel", *IEEE Transactions on Magnetics*, Vol. 26, no. 5, September, pp. 2553-2558.

Stranges, N., Findlay, R. D., 2000, "Measurement of Rotational Iron Losses in Electrical Sheet", *IEEE Transactions on Magnetics*, Vol. 36, No. 5 September, pp. 3457-3459.

Stauffer, L. H., 1952, U.S.A. Patent No 2 828 467.

Werner, E., 1949, Austrian Patent no. 191 015.

Wiley. J& Sons., 1997, Principles of Electrical Machines and Power Electronics, Second edition, John Wiley & Sons.

Young, F. J., Schenk, H. L., 1996, "Iron Losses in Elliptically Polarized Magnetic Fields", *J. Appl. Phys*, Vol. 37, No. 3, March, pp.1210-1211.

Zurek, S., Meydan, T., 2006, "Rotational Power Losses and Vector Loci Under Controlled High Flux Density and Magnetic Field in Electrical Steel Sheets," *IEEE Transactions on Magnetics*, Vol. 42, No. 10, October, pp. 2815-2817.